Journal of Cleaner Production 346 (2022) 131143

Contents lists available at ScienceDirect

Journal of Cleaner Production

journal homepage: www.elsevier.com/locate/jclepro

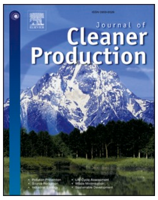

Peroxymonosulfate activation induced by spinel ferrite nanoparticles and their nanocomposites for organic pollutants removal: A review

Jingwen Sun [1], Ting Wu [1], Zhifeng Liu [*], Binbin Shao, Qinghua Liang, Qingyun He, Songhao Luo, Yuan Pan, Chenhui Zhao, Danlian Huang

College of Environmental Science and Engineering, Hunan University and Key Laboratory of Environmental Biology and Pollution Control (Hunan University), Ministry of Education, Changsha, 410082, PR China

ARTICLE INFO

Handling Editor: M.T. Moreira

Keywords:
Spinel ferrite
Sulfate radical
Advanced oxidation processes
Organic pollutant

ABSTRACT

In the face of the increasingly serious water pollution problem, sulfate radical-based advanced oxidation processes gradually developed due to their remarkable ability to degrade refractory organic pollutants. Spinel ferrite nanoparticles (NPs) and their nanocomposites (NCs) can be used as catalysts to activate peroxymonosulfate (PMS) with great catalytic performance, high stability, and reusability, which has attracted some attention of scholars in recent years. Firstly, the advantages and mechanisms of PMS activation induced by various spinel ferrite NPs and their NCs for organic pollutants removal are reviewed in this paper. Secondly, the influence factors of catalyst performance and PMS activation are discussed. Finally, the challenges of PMS activation induced by spinel ferrite NPs and their NCs are put forward and the direction of improvement is proposed.

1. Introduction

With the rapid development of industrialization and the swift growth of population, organic pollution is becoming more and more serious (Pan et al., 2020; Shao et al., 2020, 2021; Wu et al., 2020). The stable nature of refractory organic pollutants enables them to persist in the environment for a long time and bring the risk of teratogenic and carcinogenic to organisms through bioconcentration (Xiao et al., 2019). Traditional biological treatment methods are difficult to handle refractory organic pollutants. Therefore, advanced oxidation processes (AOPs), which can effectively degrade refractory organic pollutants, have become a current research hotspot.

The highly reactive radicals generated by AOPs can directly degrade most organic pollutants or increase the biodegradability of pollutants through oxidation. AOPs usually take hydroxyl radical (•OH) and sulfate radical (SO_4^-•) as the main active species. Despite hydroxyl radical-based advanced oxidation processes (HR-AOPs) having been extensively studied in recent decades, their applications are still limited due to the harsh reaction conditions, the instability of oxidants, and a large amount of sludge production. Compared with HR-AOPs, sulfate radical-based advanced oxidation processes (SR-AOPs) has the advantages of more stable active species and higher radical activity. Besides, SO_4^-• can be used to attack organic pollutants which contain unsaturated bonds or aromatic Π electrons directly via electron transfer reaction (Hu and Long, 2016). The literature on SR-AOPs covers multifarious aspects of the environmental field, such as the removal of organic pollutants from wastewater (Yang et al., 2019; Bhat and Gogate, 2021; Giannakis et al., 2021), in-situ chemical oxidation (ISCO) technology (Tsitonaki et al., 2010; Yuan et al., 2014; Zhou et al., 2018) and biodegradability improvement (Rizzo, 2011). Consequently, SR-AOPs have attracted more attention and extensive research due to their broad application prospects.

Peroxymonosulfate (PMS) (Fig. 1) is one of the major sources of SO_4^-•, and its main properties are shown in Table 1. The activation modes of PMS can be divided into two categories: homogeneous systems and heterogeneous systems. Homogeneous activations usually have problems such as high energy consumption and difficult recovery. In contrast, heterogeneous systems have greater advantages and practicability. Firstly, heterogeneous activators are convenient to separate from water for recycling and basically do not require secondary treatment. Secondly, heterogeneous systems can operate over a wide pH range (pH 2–9) and is not prone to hydrolysis and precipitation of metal ions like homogeneous systems (Fang et al., 2013; Duan et al., 2015; Oh et al., 2016).

---

[*] Corresponding author.
E-mail address: zhifengliu@hnu.edu.cn (Z. Liu).

[1] The authors contribute equally to this paper.

https://doi.org/10.1016/j.jclepro.2022.131143
Received 10 October 2021; Received in revised form 21 February 2022; Accepted 24 February 2022

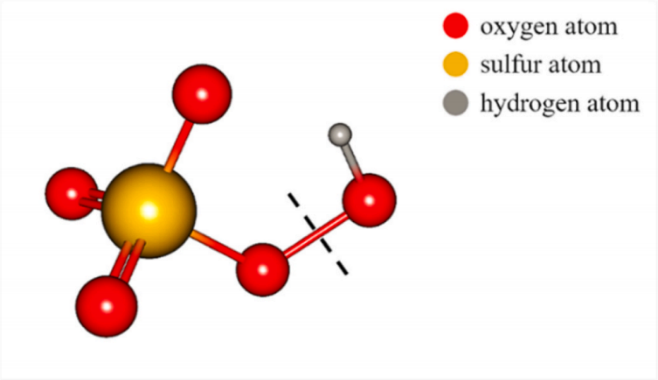

Fig. 1. The structure of PMS. HSO_5^- is the active component of PMS. The dashed line is the fission position of the O–O bond during the formation of $SO_4^-\bullet$.

Table 1
The properties of PMS.

Properties	PMS	Ref.
Chemical formula	$2KHSO_5 \cdot KHSO_4 \cdot K_2SO_4$ (Oxone®)	Ike et al. (2018)
CAS number	10058-23-8	
Standard reduction potential	1.75–1.82 V	Yu et al. (2020)
O–O bond dissociation energy (kJ/mol)	377	Benson (1978)
Solubility in water at 25 °C (g/L)	298	Kolthoff and Miller (1951)
Average estimated lifetime	hours to days	Wacławek et al. (2017)

Metal-based catalysts have been widely studied and used in heterogeneous systems for their ability to significantly improve reaction activity. As competent metallic elements, Co-, Fe-, Cu- and Mn-based catalysts have made satisfactory progress in PMS activation (Lei et al., 2015; Liu et al., 2016; Jawad et al., 2018). To further improve the properties, the researchers found that polymetallic coexistence in the catalyst could significantly promote the activation process. In this case, the research of PMS activation by ferrite NPs and their NCs has been developed. Ferrites are a class of magnetic complex oxides consisting of Fe and one or more other appropriate transition metal elements, which have the advantages of easy preparation, high specific surface areas, great chemical stability, tunable shape and size, low cost, and abundant resources (Reddy and Yun, 2016). Ferrites normally exhibit ferrimagnetism and have strong magnetic properties. Therefore, ferrites have the significant advantage of being easily recovered from the water by magnetic separation, which can effectively alleviate the problem of residue. As a stable ferrite, the spinel ferrite has received special attention and is often used as an activator for PMS activation to oxidize refractory organic pollutants due to its simple chemical composition, high catalytic activity, stable spinel structure (shown in Fig. 2), and easy recovery (Kefeni et al., 2017). On account of strong metal interaction, spinel ferrite NPs and their NCs show excellent activated ability, which is much better than single metal catalysts.

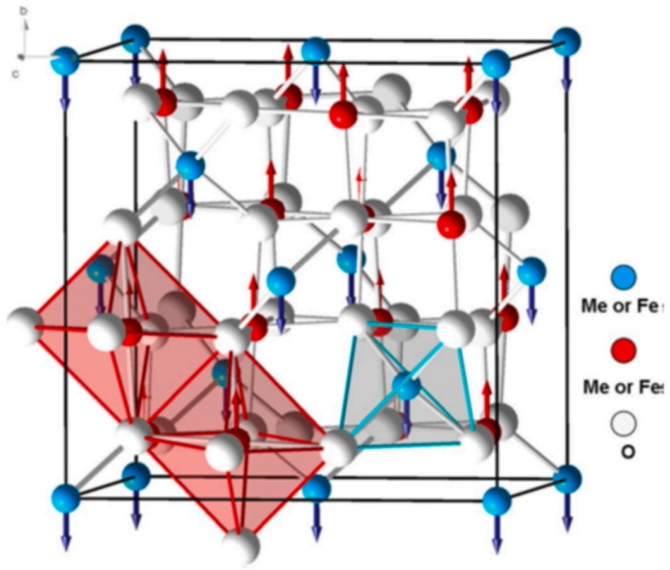

Fig. 2. Schematic diagram of spinel ferrite structure (Harris et al., 2009), Copyright 2009 Elsevier.

Until now, spinel ferrite NPs and their NCs have been widely researched for PMS activation. However, up to now, there are few comprehensive and detailed reviews have been made on PMS activation induced by various spinel ferrite NPs and their NCs for organic pollutants removal (Peng et al., 2021). To promote further development and application, it is necessary to summarize this field and provide ideas for subsequent research. With the help of "Web of Science", the latest research on spinel ferrite NPs and their NCs/PMS system in the removal of organic pollutants in the past 5 years, as well as the classic and influential research in recent years are obtained. Herein, a systematic review focuses on various spinel ferrite NPs and their NCs for organic pollutants removal in SR-AOPs is carried out. And the frequently-used synthesis methods of spinel ferrite NPs and their NCs, influence factors, and mechanisms of PMS activation are discussed. Finally, the challenges and improved direction are proposed, hoping to provide guidelines for further research.

2. Spinel ferrite nanoparticles and nanocomposites in PMS activation

2.1. Spinel ferrite magnetic nanoparticles

2.1.1. Superiorities of MFe_2O_4 NPs in PMS activation

Spinel ferrites are named because their crystal structure is the same as that of the natural mineral spinel. The chemical formula of spinel ferrites is MFe_2O_4, where M represents bivalent metal ions with a radius close to Fe^{2+} (such as Co^{2+}, Cu^{2+}, Mn^{2+}, Ni^{2+}, Zn^{2+}, etc.) or a variety of metal ion groups whose average chemical valence state is divalent. Different types of MFe_2O_4 can be prepared using different alternative metal ions. MFe_2O_4 doped with one metal ions are called single-component MFe_2O_4, while MFe_2O_4 doped with two or more metal ions are called multi-component MFe_2O_4.

In SR-AOPs, typical single-component MFe_2O_4 NPs used as PMS catalysts are $CoFe_2O_4$, $MnFe_2O_4$, $CuFe_2O_4$, and $NiFe_2O_4$. The morphology and microstructure of these MFe_2O_4 NPs are shown in Fig. 3. The surface of MFe_2O_4 NPs is irregular granular with a porous structure, which not only increases the contact area between catalysts and reactants but also enhances the catalytic performance. Nevertheless, magnetic NPs reveal a tendency of aggregation, resulting in the loss of accessible active sites, which go against the catalytic process. Some scholars have confirmed that MFe_2O_4 NPs as polymetallic catalysts have faster and better catalytic performance than single metal catalysts due to the synergistic effect (shown in Fig. 4). A virtuous cycle is formed between M^{2+}/M^{3+} and Fe^{3+}/Fe^{2+}, which accelerates the generation of radicals and promotes the smooth process of degradation. As an illustration, Cai et al. (2020) observed that the degradation efficiency of bisphenol A (BPA) under the $CoFe_2O_4$/PMS system was 96.0% in 60 min, while that of the Fe_2O_3/PMS system was only 21.6% in the same time. Moreover, Xu et al. (2016) found the degradation efficiency of BPA under $CuFe_2O_4$/PMS system was 95.2% in 60 min, while that of

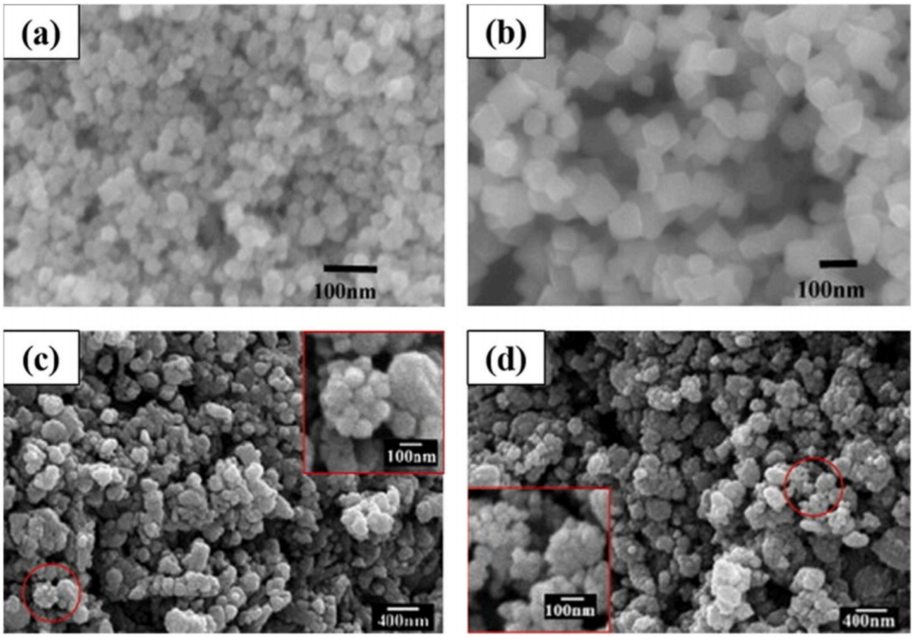

Fig. 3. SEM images of (a) $CoFe_2O_4$ and (b) $MnFe_2O_4$ (Wang et al., 2012), Copyright 2012 Elsevier. SEM images of (c) $CuFe_2O_4$ and (d) $NiFe_2O_4$ (Laokul et al., 2011), Copyright 2011 Elsevier.

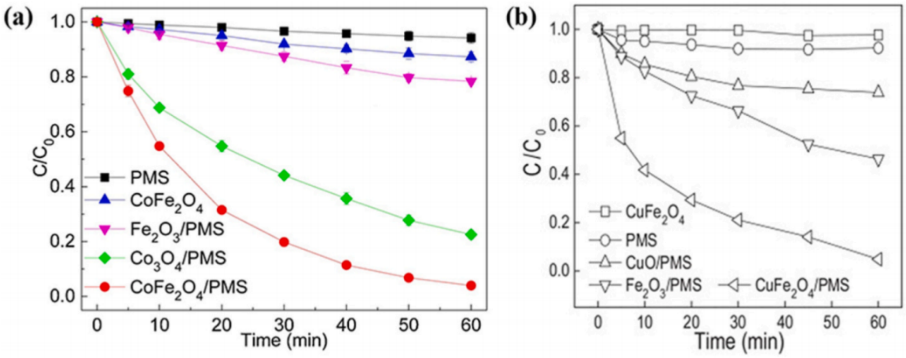

Fig. 4. Degradation of BPA under different systems: (a) [BPA] = 0.1 mM, [Catalyst] = 0.2 g/L, [PMS] = 1.0 mM, $pH_0 = 6.3$ (Cai et al., 2020), Copyright 2020 Elsevier. (b) [BPA] = 50 mg L^{-1}, [Catalyst] = 0.4 g L^{-1}, [PMS] = 0.5 g L^{-1}, $pH_0 = 6.72$ (Xu et al., 2016), Copyright 2016 Elsevier.

CuO/PMS system was only 26.1% at the same time.

Even under the same reaction conditions, varieties of single-component MFe_2O_4 NPs have diverse catalytic activities of PMS, which might be correlated with the activity of M^{2+} in the crystal phase. Ren et al. (2015) prepared different types of MFe_2O_4 (M = Co, Cu, Mn, and Zn) and observed the capacity of catalytic PMS was $CoFe_2O_4 > CuFe_2O_4 > MnFe_2O_4 > ZnFe_2O_4$. $CoFe_2O_4$ exhibited the highest catalytic effect on PMS oxidation, which was related to the abundant hydroxyl sites on the $CoFe_2O_4$ surface and the best synergistic effect of Co and Fe ions. Although the catalytic activity of $CuFe_2O_4$ and $MnFe_2O_4$ is not as high as that of $CoFe_2O_4$, Cu^{2+} and Mn^{2+} are not as likely to be a potential carcinogen as Co^{2+} (Guan et al., 2013). Besides, the cost of $MnFe_2O_4$ (2.43 dollars/100 g) is lower than that of $CoFe_2O_4$ (9.11 dollars/100 g) (Pang and Lei, 2016). Thus, $CuFe_2O_4$ and $MnFe_2O_4$ might have immeasurable feasibility for application in the industrial field.

Excellent stability and reusability are also important advantages of MFe_2O_4 NPs as competent PMS activators. Li et al. (2018) analyzed the XRD patterns of $CoFe_2O_4$ before and after reaction and peak locations of the used $CoFe_2O_4$, then found no obvious difference and valence state change happened on Fe^{3+}, indicating the catalysts are structurally stable. Pan et al. (2017) conducted ion leakage and recycle tests, then observed that the concentration of Co^{2+} and Fe^{3+} in the reaction system were far below the limit value (2.0 mg/L) of EU's "Registration, Evaluation, Authorization and Restriction of Chemicals", revealing $CoFe_2O_4$ would not induce serious secondary pollution. Owing to the relative stability of spinel structure, the leaching of metal ions from the solid phase could be markedly reduced (Zhang et al., 2013). Moreover, a study has shown that $CoFe_2O_4$ could be reusable for at least 5 cycles with very low cobalt leaching (<160 μg/L) (Cai et al., 2020), revealing its latent recyclability and favorable long-term durability.

In conclusion, MFe_2O_4 NPs have the following advantages: (a) The presence of Fe^{3+} can significantly inhibit the leaching of M^{2+} due to the strong Fe-M interaction. MFe_2O_4 NPs show great stability owing to the stable spinel structure, which is also one of the reasons for the reduction of metal leaching. (b) MFe_2O_4 NPs can be readily recycled using magnetic separation thanks to their unique ferrimagnetic properties. (c) MFe_2O_4 NPs exhibit higher surface catalytic activity than single metal catalysts, which may be attributed to the strong synergistic effect between M and Fe. Moreover, the presence of Fe is discovered to be conducive to enhancing the content of hydroxyl groups (M-OH) on MFe_2O_4 NPs surface, which is regarded to contribute to the formation of MOH^+ (Eq. (1)-Eq. (3)) (Yang et al., 2009). It is a crucial step in heterogeneous PMS activation by MFe_2O_4 NPs.

$$Fe^{3+} + H_2O \rightarrow FeOH^{2+} + H^+ \tag{1}$$

$$M^{2+} + FeOH^{2+} \rightarrow MOH^+ + Fe^{3+} \tag{2}$$

$$MOH^+ + HSO_5^- \rightarrow MO^+ + SO_4^- \bullet + H_2O \tag{3}$$

To further improve the catalytic performance and stability, some scholars used MFe_2O_4 NPs doped with different elements, namely multi-component MFe_2O_4 NPs, as catalysts for PMS activation. The influence of different element doping modifications on the catalytic performance was studied to determine the optimal doping type. For example, the $NiFe_2O_4$ and $MnFe_2O_4$ are doped by Co^{2+} or Cu^{2+} respectively to obtain different content of doped MFe_2O_4. The catalytic performance of $NiFe_2O_4$ is poor, while it is obviously improved after doping with Co^{2+}. Low concentration doping is beneficial to improve the catalytic performance of $NiFe_2O_4$, while high concentration doping will lead to lattice distortion and reduce the catalytic performance. On the contrary, for $MnFe_2O_4$, which has good catalytic performance, no matter doping Co^{2+} or doping Cu^{2+}, its catalytic effect is not significantly improved. Therefore, the improved method of element doping is more suitable for MFe_2O_4 with poor performance in the PMS activation system. Meanwhile, the metal ion selected for doping should have a similar radius to the metal to be doped, the chemical properties, as well as the ability to gain and lose electrons, should also be similar so that the structure of the doped catalyst is relatively stable.

2.1.2. Mechanism of PMS activation induced by MFe_2O_4 NPs

Activation reactions in MFe_2O_4/PMS system mainly occur on the surface of MFe_2O_4 NPs. In the reaction process, $SO_4^-\bullet$ and •OH are the main active species, which play a key role in the removal of organic pollutants. The prominent activity of MFe_2O_4 NPs is owing to the distinct synergistic effect, which is conducive to the continuous decomposition of PMS and the generation of radicals. A brief mechanism of PMS activation by MFe_2O_4 NPs is shown in Fig. 5.

Metal ions act as Lewis acids and bind to the adsorbed H_2O molecules. It leads to the formation of a large number of activated hydroxyl groups (MOH^+ and $FeOH^{2+}$) on the surface of MFe_2O_4 NPs (Eq. (4) and Eq. (1)), which is the rate-limiting step of PMS activation. As well, $FeOH^{2+}$ can furthermore react with M^{2+} to form MOH^+ (Eq. (2)). Then these hydroxyl groups are combined with HSO_5^- in the reaction solution through hydrogen bonds, and exist in the form of MFe_2O_4–O–H–HSO_5^-. MOH^+ can activate HSO_5^- to form $SO_4^-\bullet$ and MO^+ (Eq. (3)), while MO^+ could reduce HSO_5^- to MOH^+ (Eq. (5)), building a virtuous cycle of repeated MOH^+ production. In the presence of H^+, MO^+ can be oxidized to M^{3+} according to Eq. (6) and Eq. (7). Besides, Fe^{3+} on MFe_2O_4 NPs surface can activate HSO_5^- into $SO_4^-\bullet$ and $SO_5^-\bullet$ by Eq. (8) and Eq. (9). The generated $SO_4^-\bullet$ can further form •OH according to Eq. (10). The formation of radicals on the catalyst surface is an important step in the oxidation process. As strong oxidants, $SO_4^-\bullet$ and •OH lead to the degradation of organic pollutants through typical chain reactions.

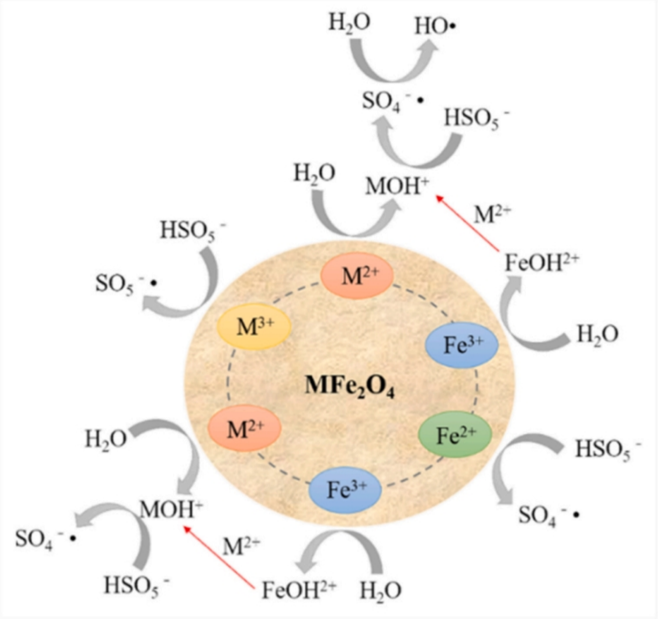

Fig. 5. Possible mechanism of PMS activation induced by MFe_2O_4 NPs.

$$M^{2+} + H_2O \rightarrow MOH^+ + H^+ \tag{4}$$

$$MO^+ + HSO_5^- \rightarrow MOH^+ + SO_5^-\bullet \tag{5}$$

$$MO^+ + 2H^+ \rightarrow M^{3+} + H_2O \tag{6}$$

$$M^{3+} + HSO_5^- \rightarrow M^{2+} + H^+ + SO_5^-\bullet \tag{7}$$

$$Fe^{3+} + HSO_5^- \rightarrow Fe^{2+} + H^+ + SO_5^-\bullet \tag{8}$$

$$Fe^{2+} + HSO_5^- \rightarrow Fe^{3+} + SO_4^-\bullet + OH^- \tag{9}$$

$$SO_4^-\bullet + H_2O \rightarrow SO_4^{2-} + HO\bullet + H^+ \tag{10}$$

Moreover, based on the standard reduction potentials of M^{3+} and Fe^{3+} (Eq. (11)-Eq. (13)), the reduction of M^{3+} by Fe^{2+} (Eq. (14)) is thermodynamically advantageous. This means that the catalyst containing both M and Fe can facilitate the regeneration of M^{2+} on the surface of MFe_2O_4 NPs. In MFe_2O_4/PMS system, the collaborative catalytic cycle of M^{2+}-M^{3+}-M^{2+} and Fe^{3+}-Fe^{2+}-Fe^{3+} is formed, which is one of the reasons why MFe_2O_4 maintains good catalytic performance. Through PMS activation, the valence states of M and Fe are reconverted to divalent and trivalent states, respectively.

$$Co^{3+} + e^- \rightarrow Co^{2+} \quad E^0 = 1.81\ V \tag{11}$$

$$Cu^{3+} + e^- \rightarrow Cu^{2+} \quad E^0 = 1.57\ V \tag{12}$$

$$Fe^{3+} + e^- \rightarrow Fe^{2+} \quad E^0 = 0.77\ V \tag{13}$$

$$Fe^{2+} + M^{3+} \rightarrow Fe^{3+} + M^{2+} \tag{14}$$

2.2. Supported spinel ferrite nanocomposites

Composites can often combine the advantages of different materials and reduce some drawbacks to achieve better performance and catalytic effect. By loading MFe_2O_4 NPs onto a support to form MFe_2O_4 NCs, the stability of the catalyst can be further enhanced (Zhang et al., 2016, 2020; Ma et al., 2020). In addition, the active site can be dispersed to a certain extent and the agglomeration of magnetic NPs can be relieved (Dong et al., 2019).

2.2.1. Carbon-derived supports

Carbon-derived materials are broadly employed as supports in PMS activation due to their superior controllability, high stability, and low leaching. The large specific surface area, developed porous structure, and abundant surface functional groups of carbon-derived materials are not only conducive to adsorb organic matter but also supply more active sites for reactions that occur on the surface of catalysts. As outstanding supports, carbon-derived materials can maintain the dispersion of NPs and the separation of charge. In addition, the introduction of magnetic MFe_2O_4 NPs enabled catalysts to be easily separated by magnetic separation. Meanwhile, carbon-derived materials are also dependable PMS activators (Xiao et al., 2018; Peng et al., 2020). They are accompanied by catalytic reactions in many adsorption processes and show catalytic activity (Yao et al., 2019).

Some scholars prepared MFe_2O_4/biochar (BC) magnetic NCs and applied them to the catalyst/PMS system (Fu et al., 2019; Zhao et al., 2020). Li et al. (2020) loaded $CoFe_2O_4$ NPs with BC and fabricated $CoFe_2O_4$/BC with strong magnetic properties, hierarchical porous and graphitized structure, emphasizing the synergistic effect between graphitized structure and $CoFe_2O_4$. They observed that although the mass percentage of $CoFe_2O_4$ in $CoFe_2O_4$/BC was only 10%, the BPA removal efficiency by $CoFe_2O_4$/BC/PMS system was significantly better than that of pure $CoFe_2O_4$/PMS system under the same reaction conditions. This phenomenon can be related to the positive promoted effect between graphitized structure and $CoFe_2O_4$ NPs (shown in Fig. 6a). It was found that the graphitized structure was conducive to PMS activation, and the graphitization process could convert amorphous carbon into graphitized carbon, which enhances the charge density of nearby carbon atoms, accordingly promoting electron transfer and producing more active catalytic sites (Tian et al., 2018). Carbon-derived materials with graphitized structures could realize a non-radical pathway by mediating the transfer of electrons from pollutants as electron donors to PMS as electron acceptors (shown in Fig. 6b).

The interatomic force of graphene is very strong and it has a stable lattice structure. Graphene can not only offer attachment sites for MFe_2O_4 NPs but also improve the efficiency of electron transfer. As popular carbon-derived materials, graphene-based materials have attracted extensive attention from researchers because of their excellent performance and great potential in improving the properties of MFe_2O_4 NPs in SR-AOPs (Yao et al., 2014a,b; Xu et al., 2019; Hao et al., 2020). Xu et al. (2015) found graphene-based $CoFe_2O_4$ (G-$CoFe_2O_4$) was more efficient than $CoFe_2O_4$ in PMS activation. Under the same reaction conditions, it only took 45 min for G-$CoFe_2O_4$/PMS system to completely degrade dimethyl phthalate, while the $CoFe_2O_4$/PMS system took twice the time. Graphene in these NCs acted as a substrate rather than a catalyst to adsorb organic pollutants. Graphene oxide (GO) is one of the important derivatives of graphene. The introduction of oxygen-containing functional groups not only makes GO chemically stable but also provides surface-modified active sites and large specific surface areas. In the process of composite with MFe_2O_4, GO can effectively disperse the attached materials and prevent agglomeration. Chen et al. (2018a,b) synthesized $CoFe_2O_4$-GO coupled with PMS for norfloxacin removal. Under appropriate reaction conditions, norfloxacin can be completely degraded, revealing its excellent performance in activating PMS for organic pollutants removal. And GO did not only function as support here, but the surface oxygen species at its defective sites played a vital role in the degradation system.

2.2.2. *Water treatment residuals and sludge-derived supports*

Nowadays, with the shortage of resources, the technology and method of treating waste by waste have gained increasing attention from scholars. Water treatment residues (WTRs) often contain metal elements with catalytic properties, making them potential feedstock of metals, which can reduce resource consumption and costs. Sludges are carbonaceous, and the carbon material derived from them often has a microporous structure and provides a large specific surface area for the diffusion of reactants to the active site. Moreover, after treatment and processing, WTRs and sludges can become the supports of MFe_2O_4, promoting the uniform distribution of NPs and preventing the occurrence of aggregation phenomena.

Li et al. (2019) employed WTRs as potential Fe source and catalyst support of $CoFe_2O_4$ and suggested the high efficiency of $CoFe_2O_4$@WTRs as PMS activator in degradation of atrazine. Under the optimum reaction conditions, the removal efficiency of atrazine can be up to 98.2% in $CoFe_2O_4$@WTRs/PMS system. Yang et al. (2020) fabricated sludge-derived activated carbon and used it as a support for $CoFe_2O_4$. Experimental results showed that $CoFe_2O_4$-SAC/PMS system was superior to $CoFe_2O_4$/PMS system in the degradation process. The unique structure of SAC relieved magnetic $CoFe_2O_4$ NPs from aggregation partially. Furthermore, the high graphitized carbon could transfer electrons rapidly and had abundant structural defects, which might facilitate the transportation of unpaired electrons, leading to the generation of radicals (Zhang et al., 2010).

2.2.3. *Natural minerals*

Natural minerals are frequently-used as adsorbents catalysts or supports to remove organic pollutants due to their abundant resources, low cost, numerous surface groups, and strong stability in recent years (Li et al., 2018; Mukhopadhyay et al., 2020). Kaolinite is one of the common natural minerals with abundant aluminum hydroxyl groups and an eternal negative charge, which can prevent the agglomeration of MFe_2O_4 NPs by weakening the crystallization on the catalyst surface. Dong et al. (Dong et al., 2019) noted the outstanding strengths of kaolinite as support and prepared $CuFe_2O_4$/kaolinite NCs for efficient degradation of BPA. Fig. 7a–c distinctly shows the positive effect of kaolinite on avoiding agglomeration. $CuFe_2O_4$ NPs are evenly distributed on the surface of kaolinite, which means more exposure to the accessible active sites. Additionally, the aluminum hydroxyl groups on the surface of kaolinite can be considered as active sites for PMS activation (Li et al., 2019). Under the dual action of $CuFe_2O_4$ and kaolinite, the degradation efficiency of BPA can reach more than 98% in 60 min. The formation of $SO_4^{-}\bullet$ is not only related to the high-valence metal ion (Cu (III)) but also induced by abundant hydroxyl groups on the surface of kaolinite (shown in Fig. 7d). In addition, Wu et al. (2019) employed organo-montmorillonite (OMt) as support for $CoFe_2O_4$ and investigated the degradation efficiency of carbamazepine (CBZ) by different PMS systems. Montmorillonite is a kind of low-cost and abundant natural material, which has wonderful specific surface areas and outstanding cation exchange capacity (Liang and Li, 2017). OMt is modified from montmorillonite with stronger hydrophobicity and greater layer spacing (Lu et al., 2014). In $CoFe_2O_4$/OMt/PMS system, Co^{2+}/Co^{3+} and Fe^{2+}/Fe^{3+} actively participate in the activation of PMS without significant changes in composition (shown in Fig. 7e).

2.2.4. *Mechanism of PMS activation induced by MFe_2O_4 NCs*

In fact, it is difficult to determine whether MFe_2O_4 NCs certainly induce radical pathways or non-radical pathways. Radical and non-

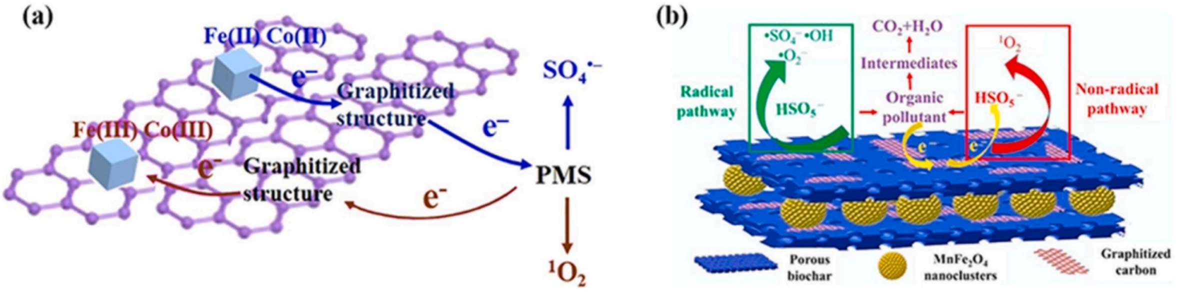

Fig. 6. (a) The synergistic effect between graphitized structure and $CoFe_2O_4$ NPs (Li et al., 2020), Copyright 2020 Elsevier. (b) Mechanism of PMS activation induced by $MnFe_2O_4$/MS for organic oxidation (Fu et al., 2019), Copyright 2019 Elsevier.

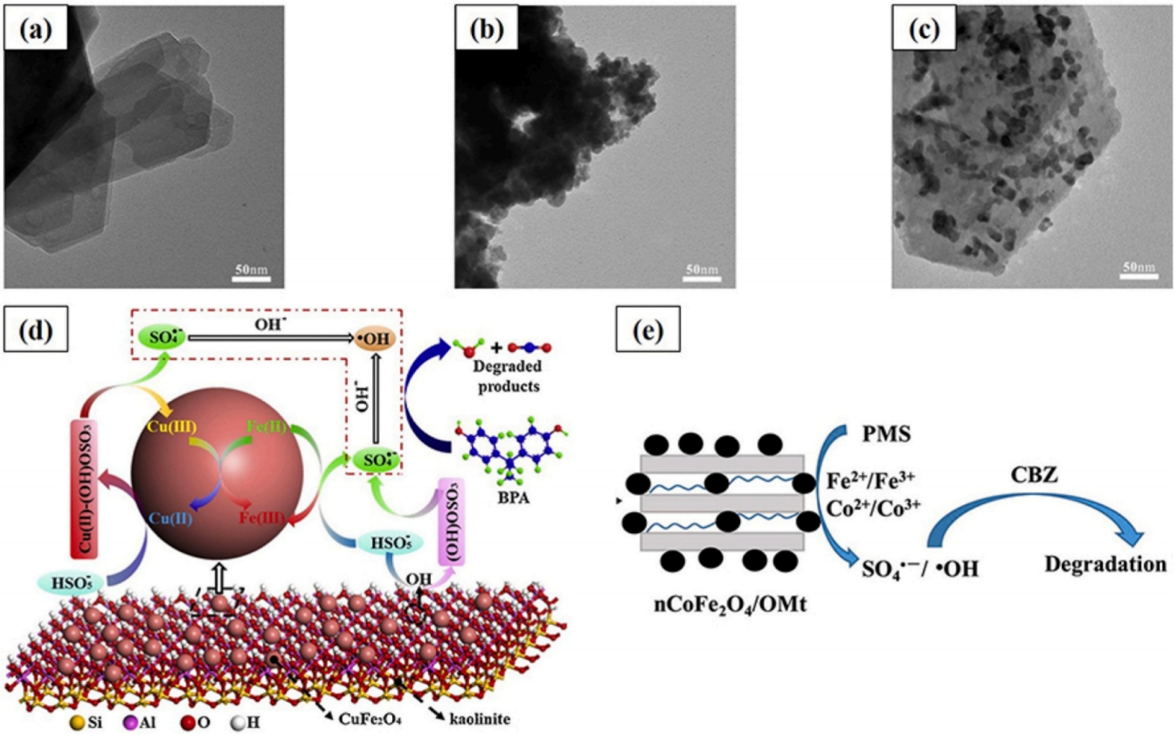

Fig. 7. TEM images of (a) kaolinite, (b) bare $CuFe_2O_4$, (c) 40%-$CuFe_2O_4$/kaolinite NCs; (d) Possible mechanism of radical generation and transfer in $CuFe_2O_4$/kaolinite/PMS system (Dong et al., 2019), Copyright 2019 Elsevier. (e) Diagram of PMS activation in $CoFe_2O_4$/OMt system (Wu et al., 2019), Copyright 2019 Elsevier.

radical pathways may occur simultaneously or independently. The specific pathway is related to the type, functional groups, and defect degree of supports.

In the radical pathway, the O–O bond of PMS will break, splitting it into two parts. A part of them receives electrons from electron donors and releases as ions (SO_4^{2-} and OH^-). The remaining part with unpaired electrons is called radicals ($SO_4^-\bullet$ and $\bullet OH$).

In the non-radical pathway, the O–O bond of PMS will not be broken, but it is stretched to generate surface-active complex, which can straight attack pollutants or further react with $OH^-/H_2O/O_2$ to produce $^1O_2$. The attack of the surface-active complex on organic pollutants can be divided into two types: (1) PMS and pollutants are adsorbed at same or similar locations on the surface of the support. The ternary system of PMS/pollutant/support is formed, and the unbalanced electron distribution leads to electron transfer in the structure. This allows the surface-active complex to further oxidize the adsorbed organic pollutants through rapid electron transfer rather than releasing radicals. (2) PMS and pollutants are adsorbed at different locations on the surface of the support. PMS is far from pollutants and direct electron transfer between them is difficult. This is where the support played a crucial role. For example, the lattice of carbon-derived materials can facilitate electron shuttle and accelerate electron transfer from pollutants to PMS.

2.3. Synthesis methods

At present, the frequently-used synthesis methods of MFe_2O_4 NPs and NCs mainly include sol-gel method, co-precipitation method, hydrothermal method, and template method. In practice, these methods are generally combined or modified to obtain better products with improved properties. Table 2 shows the synthesis methods of various MFe_2O_4 NPs and NCs, and Fig. 8 displays the preparation processes by different synthesis methods.

MFe_2O_4 NPs preparation by sol-gel method involves adding the aqueous solution of Fe and M salts to an additive solution (such as citric acid or egg white) drop by drop. Then evaporating the mixture in a water bath to form a gel, which will be calcinated to obtain MFe_2O_4 NPs (Zhao et al., 2018). It has been proved that the sol-gel combustion method can effectively accommodate different cations in the complex and make the cations uniformly mixed (Ding et al., 2013). The raw materials used in the sol-gel method are first dispersed into the solvent to form a low-viscosity solution, which makes it easy to obtain uniformity at the molecular level.

Co-precipitation method has the advantages of simple process, easy control of preparation conditions, and short synthesis period. NaOH is a frequently-used precipitant, MFe_2O_4 NPs and NCs can be obtained by adding it to the pre-prepared mixed metal salt solution without complicated processing (Senapati et al., 2011). However, in the process of preparing MFe_2O_4 NPs by co-precipitation, every stage may lead to the formation of agglomerates, which will reduce the catalytic performance of obtained materials. Supports with remarkable nature can effectively alleviate NPs agglomeration.

Compared with sol-gel method and co-precipitation method, the biggest advantage of hydrothermal method is that the crystalline products can be obtained directly without calcination, avoiding the formation of particle agglomeration. Hydrothermal method takes an aqueous solution as the reaction system and heats the mixed salt solution of Fe and M in an autoclave. The temperature difference in the autoclave is controlled to generate convection, so that the solution reaches a supersaturated state, then products are synthesized and processed by recrystallization.

Template method is used to synthesize ordered mesoporous or porous MFe_2O_4 NPs, which can effectively prevent self-aggregation and provide more active sites. Through the physicochemical interaction, precursors are formed in the cavity of the template. After extraction, oxidation, or calcination, products with ordered mesoporous or porous structures can be obtained from the template.

Table 2
Synthesis methods of various MFe_2O_4 NPs and NCs.

Material	Synthesis method	Raw materials	Characteristics	Ref.
MFe_2O_4 (M = Co, Cu, Mn, and Zn)	Sol-gel process with egg white	$Co(NO_3)_2{\cdot}6H_2O$, $Cu(NO_3)_2{\cdot}3H_2O$, $Mn(NO_3)_2{\cdot}50\%$, $Zn(NO_3)_2{\cdot}6H_2O$ and $Fe(NO_3)_3{\cdot}9H_2O$.	The average crystallite size of MFe_2O_4 ranges between 18 nm and 44 nm.	(Ren et al., 2015)
$CuFe_2O_4$, $NiFe_2O_4$ and $ZnFe_2O_4$	Modified sol-gel method using high purity metal nitrates and aloe vera plant extracted solution.	$Ni(NO_3)_2{\cdot}6H_2O$, $Cu(NO_3)_3{\cdot}3H_2O$, $Zn(NO_3)_2{\cdot}6H_2O$, $Fe(NO_3)_3{\cdot}9H_2O$ and aloe vera extract solution.	Crystallite size is 15–70 nm.	(Laokul et al., 2011)
MFe_2O_4 (M = Mn, Fe, Co, Ni)	Hydrothermal method	$FeSO_4{\cdot}7H_2O$ or $FeCl_3{\cdot}6H_2O$ and MCl_2 (M = Mn, Co, Ni).	NPs diameter is about 10–20 nm ($NiFe_2O_4$), 80–100 nm ($MnFe_2O_4$) and 30–40 nm ($CoFe_2O_4$).	(Wang et al., 2012)
$(Fe_{3-x}Mn_x)_{1-\delta}O_4$ (x = 0, 0.2 and 0.5)	Co-precipitation method	Ferrous sulfate, ferric chloride, and manganese sulfate.	BET surface areas: 88.5 (x = 0), 68.0 (x = 0.2) and 101 (x = 0.5) $m^2\ g^{-1}$.	Yang et al. (2011)
$CoFe_2O_4$	Modified sol-gel combustion method	$Co(NO_3)_2{\bullet}6H_2O$ and $Fe(NO_3)_3{\bullet}9H_2O$.	The values of BET specific surface area, total pore volume and mean pore diameter are 59.5 m^2/g, 0.2 cm^3/g, and 12.8 nm, respectively.	(Cai et al., 2020)
$CoFe_2O_4$	Hydrothermal method	$Co(NO_3)_2{\cdot}6H_2O$ and $Fe(NO_3)_3{\cdot}9H_2O$.	NPs with an average size of about 13 nm.	(Li et al., 2018)
$CuFe_2O_4$	Sol-gel combustion method	$Cu(NO_3)_2{\cdot}3H_2O$ and $Fe(NO_3)_3{\cdot}9H_2O$.	Quasi-sphere particles with particle sizes of about 100 nm.	Ding et al. (2013)
$CuFe_2O_4$	Through the nanocasting strategy, using the as-prepared KIT-6 as hard templates.	$Cu(NO_3)_2{\cdot}6H_2O$, $Fe(NO_3)_3{\cdot}9H_2O$, and KIT-6.	Well-ordered mesoporous structure; Pore size is 2.3 nm.	Wang et al. (2014)
$CoFe_2O_4$@WTRs	Modified chemical co-precipitation combined with calcination method.	$Co(NO_3)_2{\cdot}6H_2O$ and drinking water treatment residuals (WTRs).	The average pore size is 19.94 nm; the specific surface area is 18.82 $m^2\ g^{-1}$.	(Li et al., 2019)
AC@$CoFe_2O_4$	Facile co-precipitation method	$Fe(NO_3)_3{\bullet}9H_2O$, $Co(NO_3)_2{\bullet}6H_2O$, and AC.	Light-colored shell and the dark-colored core; Nano-size: 5–20 nm.	(Ma et al., 2020)
$CuFe_2O_4$/MWCNTs	Sol-gel combustion method	$Cu(NO_3)_2{\bullet}3H_2O$, $Fe(NO_3)_3{\bullet}9H_2O$, and MWCNTs-COOH.	Highly stable skeleton and pore structure; Specific surface area is 40 $m^2\ g^{-1}$.	(Zhang et al., 2016)
$MnFe_2O_4$/MX (X = stems (S), leaves (L) and cores (C))	Solvothermal method	$Fe(NO_3)_3{\cdot}9H_2O$, $MnCl_2{\cdot}4H_2O$ and corn biomass (stems (S), leaves (L), and cores (C)).	NPs diameter is 50–200 nm; the surface areas are 389, 535 and 270 m^2/g for $MnFe_2O_4$/MS, $MnFe_2O_4$/ML and $MnFe_2O_4$/MC, respectively.	(Fu et al., 2019)
$CoFe_2O_4$-EG	Co-precipitation method	$Co(NO_3)_2{\cdot}6H_2O$, $Fe(NO_3)_3{\cdot}9H_2O$, and expanded graphite.	The BET specific surface area and single-point total pore volume are 38.36 m^2/g and 0.20 cm^3/g, respectively.	(Xu et al., 2019)
$CuFe_2O_4$/kaolinite	Facile citrate combustion method	$Cu(NO_3)_2{\cdot}2.5H_2O$, $Fe(NO_3)_3{\cdot}9H_2O$ and kaolinite.	The diameter is 10–20 nm; Pore size distribution is mainly in the range from 2 to 6 nm.	(Dong et al., 2019)
$CuFe_2O_4/Bi_2O_3$	Simple sol-gel combustion method	$Fe(NO_3)_3{\cdot}9H_2O$, $Cu(NO_3)_2{\cdot}3H_2O$, and $Bi(NO_3)_3{\cdot}5H_2O$.	NPs with rough surface and agglomeration; Surface area is 78.088 m^2/g,	(Zhang et al., 2020)
$CuO/Fe_2O_3/CuFe_2O_4$	Simple one-step hydrothermal method	$FeCl_3{\cdot}6H_2O$ and $CuSO_4{\cdot}5H_2O$.	All the samples consist of nanoparticles (10–30 nm) and nanoplates (about 100 nm).	Lyu et al. (2020)
$CuO/MnFe_2O_4$	Co-precipitation method	$Fe(NO_3)_2{\cdot}9H_2O$, $Mn(NO_3)_2{\cdot}4H_2O$, and $Cu(NO_3)_2{\cdot}3H_2O$.	A mixture of bumpy micropolyhedrons and nanoparticles.	Ma et al. (2019)

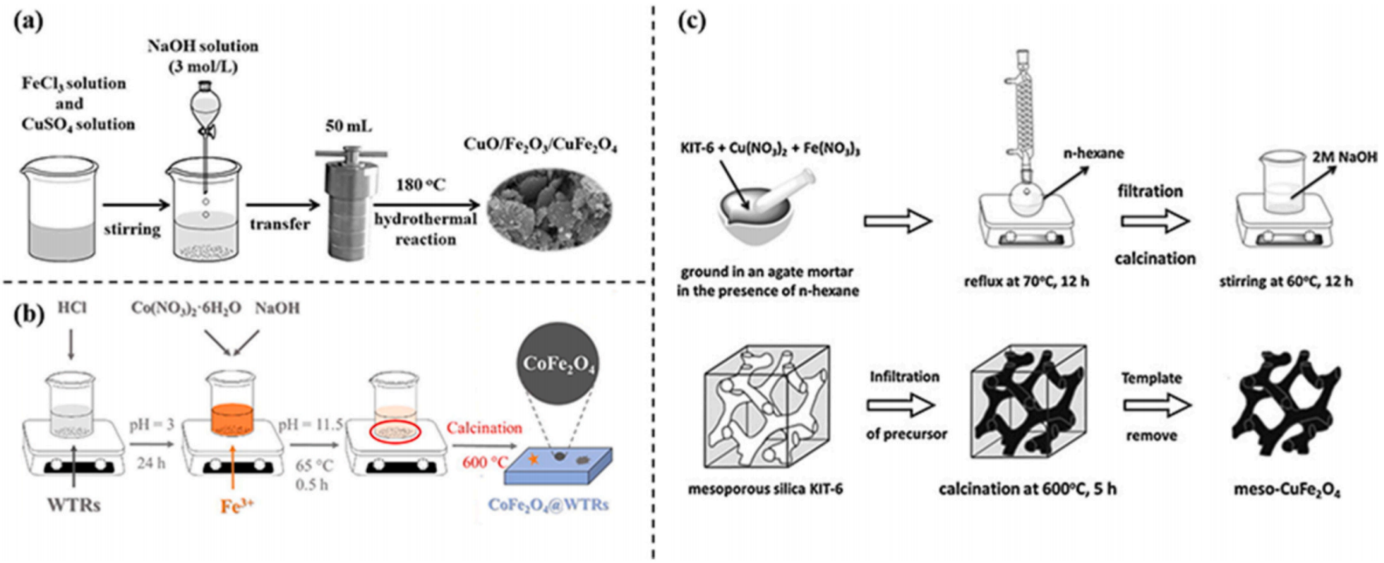

Fig. 8. The preparation processes of MFe_2O_4 NPs and NCs by different synthesis methods: (a) $CuO/Fe_2O_3/CuFe_2O_4$ preparation by hydrothermal method (Lyu et al., 2020), Copyright 2020 Elsevier. (b) $CoFe_2O_4$@WTRs preparation by co-precipitation method (Li et al., 2019), Copyright 2019 Elsevier. (c) $CuFe_2O_4$ preparation by template method (Wang et al., 2014), Copyright 2014 Elsevier.

2.4. Application in removing organic pollutants from wastewater

MFe_2O_4 NPs and NCs have been broadly used to remove organic pollutants in various wastewater because of their prominent catalytic activity to PMS, strong stability, and convenient reusability. Table 3 shows the degradation of organic pollutants by different MFe_2O_4 NPs and NCs/PMS systems.

With the development of industry, the treatment of wastewater containing phenols and dyes has become a thorny problem, because they are a kind of highly concentrated organic wastewater that is difficult to be biodegraded. It has been proved that MFe_2O_4 NPs and NCs play an energetic role in phenol-containing and dye-containing wastewater treatment (Ding et al., 2013; Yao et al., 2014a, 2014b; Du et al., 2016; Dong et al., 2019; Fu et al., 2019; Cai et al., 2020; Li et al., 2020). Organic pollutants are attacked by reactive oxygen species generated by the activation process of PMS, resulting in a variety of degradation intermediates, which are further converted into CO_2 and H_2O (Li et al., 2020; You et al., 2021).

Nowadays, the environmental pollution caused by drug residues has also attracted the great attention of scholars. Pharmaceuticals or their metabolites that are not fully absorbed and utilized can enter water bodies, which will pose a threat to ecological safety and human health. Antibiotics and pesticides are two classes of pharmaceuticals that are most widely employed in clinical treatment and practical application. And there has been evidence that MFe_2O_4 NPs and NCs/PMS systems can effectively remove residual antibiotics and pesticides in wastewater (Wang et al., 2017; Chen et al., 2018a, 2018b; Li et al., 2018; Li et al., 2019; Xu et al., 2019; Yang et al., 2020; Liu et al., 2021; Zhang et al., 2022).

Landfill leachate is high-concentration organic wastewater formed in landfills that can penetrate the ground, causing soil and groundwater pollution. Karimipourfard et al. researched the application of magnetic $CuFe_2O_4$/rGO (Karimipourfard et al., 2019) and $CuFe_2O_4$ (Karimipourfard et al., 2020) as PMS activators in landfill leachate

Table 3
Degradation of organic pollutants by various MFe_2O_4 NPs and NCs/PMS systems.

Material	Contaminant	Reaction conditions	Degradation performance	Ref.
MFe_2O_4 (M = Co, Cu, Mn, and Zn)	Dibutyl phthalate (DBP)	[PMS] = 20 μmol L^{-1}, [catalyst] = 0.1 g L^{-1}, $[DBP]_0$ = 2 μmol L^{-1}, pH = 7.0, time = 30 min.	Removal efficiency: 81.0%($CoFe_2O_4$), 62.3% ($CuFe_2O_4$), 42.3%($MnFe_2O_4$) and 30.0% ($ZnFe_2O_4$).	(Ren et al., 2015)
$CoFe_2O_4$ and $MnFe_2O_4$	Paracetamol	$[APAP]_0$ = 0.066 mM, $[PMS]_0$ = 0.20 mM, m $(MnFe_2O_4)_0$ = m$(CoFe_2O_4)_0$ = 0.2 g/L, initial pH = 4.3, time = 120 min.	TOC removal efficiency: 16.2%($CoFe_2O_4$) and 3.5%($MnFe_2O_4$); APAP removal efficiency: 90.5%($CoFe_2O_4$) and 90.5% ($MnFe_2O_4$).	Tan et al. (2017)
$CoFe_2O_4$	Bisphenol A (BPA)	[BPA] = 0.1 mM, [PMS] = 1.0 mM, [$CoFe_2O_4$] = 0.2 g/L, pH = 6.3, time = 60 min.	Removal efficiency >95%.	(Cai et al., 2020)
$CoFe_2O_4$	Atrazine	$[ATZ]_0$ = 10 mg/L, $[CoFe_2O_4]_0$ = 0.4 g/L, $[PMS]_0$ = 0.8 mM, pH = 6.3, time = 30 min.	Removal efficiency: > 99%.	(Li et al., 2018)
$CuFe_2O_4$	Iopromide	$CuFe_2O_4$ dose = 100 mg L^{-1}, initial iopromide concentration = 1 μM, PMS dose = 20 μM, pH = 6.0, T = 20 °C, time = 10 min.	Removal efficiency: up to 70%.	Zhang et al. (2013)
$CuFe_2O_4$	Tetrabromobisphenol A	initial TBBPA concentration = 10 mg L^{-1}, initial PMS concentration = 0.2 mmol L^{-1}, catalyst load = 0.1 g L^{-1}, time = 30 min.	TBBPA removal efficiency: 99%.	(Ding et al., 2013)
$CoFe_2O_4$@WTRs	Atrazine	[ATZ] = 10 μM, [PMS] = 0.25 mM, [catalyst] = 0 .03 g L^{-1}, pH = 4.01, time = 20 min.	ATZ removal efficiency: 98.2%.	(Li et al., 2019)
$MnFe_2O_4$/MX (X = stems (S), leaves (L) and cores (C))	Orange II	$[PMS]_0$ = 0.5 g/L, $[Catalyst]_0$ = 0.05 g/L, $[MnFe_2O_4/MX]_0$ = 0.05 g/L, $[orange\ II]_0$ = 20 mg/L, initial pH = 5.8, time = 6 min.	Removal efficiency: 93% (ML), 90% (MS) and 93% (MC).	(Fu et al., 2019)
$CoFe_2O_4$-EG	Sulfamethoxazole (SMX)	[SMX] = 10 mg/L, [Catalyst] = 0.6 g/L, [PMS] = 0.4 mM, pH = 6.0 ± 0.3, time = 20 min.	Removal efficiency: > 99%.	(Xu et al., 2019)
$CuFe_2O_4$/kaolinite	Bisphenol A	C_0(BPA) = 50 mg L^{-1}, C_0(PMS) = 0.5 mM, C_0(Catalyst) = 0.5 gL^{-1}, initial pH = 7.0, time = 60 min.	Removal efficiency: > 98%.	(Dong et al., 2019)
$CoFe_2O_4$/OMt	Carbamazepine (CBZ)	[catalyst] = 0.4 g L^{-1}, [CBZ] = 5 mg L^{-1}, [PMS] = 0.5 mM, pH = 6.8, time = 60 min.	Removal efficiency: 93%.	(Wu et al., 2019)
$CoFe_2O_4$/BC	Bisphenol A	$[PMS]_0$ = 0.5 g/L, $[Catalyst]_0$ = 0.05 g/L, $[BPA]_0$ = 10 mg/L, initial pH = 7.4, time = 8 min.	Removal efficiency: > 98%.	(Li et al., 2020)
$CuFe_2O_4$@Biochar	o-nitrochlorobenzene	[o-NCB] = 500 mg/kg, [PS] = 0.1 mol/L, [catalysts] = 12 mg/g, initial pH = 7.3, soil moisture = 1.0 mL/g, time = 24h.	Removal efficiency: 42%.	(Zhao et al., 2020)
G-$CoFe_2O_4$	Dimethyl phthalate (DMP)	$[PMS]_0$ = 2.0 mM, [catalyst] = 0.5 g/L, $[DMP]_0$ = 0.05 mM, time = 45 min.	Removal efficiency: almost 100%.	(Xu et al., 2015)
$MnFe_2O_4$-rGO	Orange II	[Orange II] = 20 mg/L, [PMS] = 0.50 g/L, [catalyst] = 0.050 g/L, time = 120 min.	Removal efficiency: 90%.	(Yao et al., 2014a, 2014b)
$CoFe_2O_4$-GO	Norfloxacin (NOR)	[NOR] = 15 μM, [Oxone] = 0.5 mM, [$CoFe_2O_4$-GO] = 0.3 g/L, pH = 7, time = 20 min.	Removal efficiency: almost 100%.	(Chen et al., 2018a, 2018b)
NS-CNTs/$CuFe_2O_4$	Phenylbenzimidazole-5-sulfonic acid (PBSA)	initial PBSA concentration = 5 mg/L, catalyst dose = 50 mg/L, pH = 7.0 ± 0.2, the molar ratio of PBSA to PMS 1:50, time = 40 min.	Removal efficiency: 100%.	Zhang et al. (2017)
$CoFe_2O_4$-SAC	Norfloxacin	[NOR] = 10 mg/L, [PMS] = 0.15 g/L, [catalyst] = 0.1 g/L, time = 60 min.	Removal efficiency: > 92%.	(Yang et al., 2020)
$CoFe_2O_4$/TNTs	Rhodamine B (RhB)	$[RhB]_0$ = 100 mg/L, volume (RhB) = 50 mL, [oxone] = 4.0 g/L, catalyst amount = 0.021 g, time = 30 min.	Removal efficiency: 100%.	(Du et al., 2016)
$CoFe_2O_4$/Al_2O_3	Sulfachloropyridazine (SCP)	[SCP] = 5 mg/L, [PMS] = 0.5 mM, [$CoFe_2O_4$/Al_2O_3] = 1.0 mM, initial pH = 7.00, time = 15 min.	Removal efficiency: 97.8%.	(Wang et al., 2017)

remediation. Under the optimal reaction conditions, the final removal efficiency of COD by the catalyst/PMS system could reach 65.1% and 57%, respectively.

2.5. Combination with other treatment technologies

As effective methods to remove organic pollutants, ozonation (Wang and Chen, 2020; Wu et al., 2021), photocatalysis (Guo et al., 2019; Bie et al., 2021), and external energy (Yao et al., 2021) have also received extensive attention and research by scholars. Ozonation can play an important role in the disinfection of water and wastewater and the removal of organic matter from sewage (Wang and Chen, 2020). As a strong oxidant, ozone reacts quickly with pollutants and does not produce secondary pollution. However, the solubility of ozone in water is low and the operating cost of ozonation is high. Photocatalysis has developed rapidly in recent years due to mild reaction conditions and strong oxidative ability. The photocatalyst generates radicals under light to oxidize organic pollutants (Lang et al., 2014). Nevertheless, the issue of light transmittance needs to be considered. The wastewater containing suspended solids and deep chroma is not conducive to photocatalytic reaction. External energy usually involves ultrasonic or UV/visible irradiation, which is a means of enhancing oxidation and improving efficiency. As an auxiliary means, it has a "synergistic effect" with other oxidation technologies.

As mentioned above, the highly active radicals (SO_4^{-}• and •OH) generated by SR-AOPs can oxidize macromolecular refractory organics into low-toxic or non-toxic micromolecular substances. Various MFe_2O_4 NPs and NCs/PMS systems showed satisfactory performance in removing organic pollutants from wastewater or landfill leachate. However, SO_4^{-}• is less selective and can react with most substances in water, resulting in partial loss of oxidative capacity. To effectively remove organic pollutants, it is often necessary to add a large amount of persulfate, which will cause many sulfate ions to remain in the water. Multi-technology combination is a way to reduce costs and pollution while increasing treatment efficiency. Coupled photocatalytic and persulfate oxidation system has been proved to be a promising degradation strategy of organic pollutants (Yang et al., 2019; Yang et al., 2021). Golshan et al. (2018) investigated the photo-oxidation efficiency of the TiO_2@$CuFe_2O_4$/UV/PMS system and the system showed an excellent catalytic performance in real environmental samples. Yao et al., 2014a, b) evaluated the catalytic activity of the $ZnFe_2O_4$-rGO/PMS system for the oxidative decomposition of organic dyes under visible light irradiation. The synergistic effect between photocatalysis and persulfate activation is an effective way to remove organic pollutants (Chen et al., 2021). External energy plays a direct or indirect role in PMS activation (Takdastan et al., 2018). UV can stimulate the breaking of peroxide bonds and promote the generation of radicals, while visible light irradiation can promote electron transfer between organic pollutants and catalyst/PMS. In addition, ultrasonic irradiation can directly activate PMS to generate radicals.

3. Influence factors of catalyst performance and PMS activation

3.1. pH

The pH of the reaction system can affect the activity, stability, oxidation potential, or surface charge of MFe_2O_4 NPs and NCs (Liang et al., 2007). It is well accepted that the activation energy is different under different pH conditions, and different catalytic systems require different optimal pH values (Ahn et al., 2016). It should be noted that most MFe_2O_4 NPs and NCs can play a role in a wide pH range and have a good application prospect in theory. In general, the degradation efficiency decreases with the increase of pH value, and the over-alkaline condition is not conducive to the catalytic reaction (shown in Fig. 9a). Under over-alkaline conditions ($pH > 10$), OH^{-} has a significant scavenging effect on SO_4^{-}•, which converts it into •OH (Eq. (15)). Since the oxidative capacity of •OH is not as good as that of SO_4^{-}•, the degradation efficiency is decreased relatively. Meanwhile, it has been reported that metal hydroxides can be produced under high pH, resulting in a decrease in oxidation potential and catalytic activity (Chan and Chu, 2009). The precipitation of metal hydroxides will cause a large amount of sludge, leading to secondary pollution. Moreover, there is evidence that metallic catalysts are unstable under over-acidic conditions, and the leaching of metal ions at low pH will cause secondary contamination, which will hinder the reuse of the catalyst (Lei et al., 2015).

$$SO_4^{-}\bullet + OH^{-} \rightarrow SO_4^{2-} + HO\bullet \tag{15}$$

3.2. Temperature

Reaction temperature is one of the important factors affecting

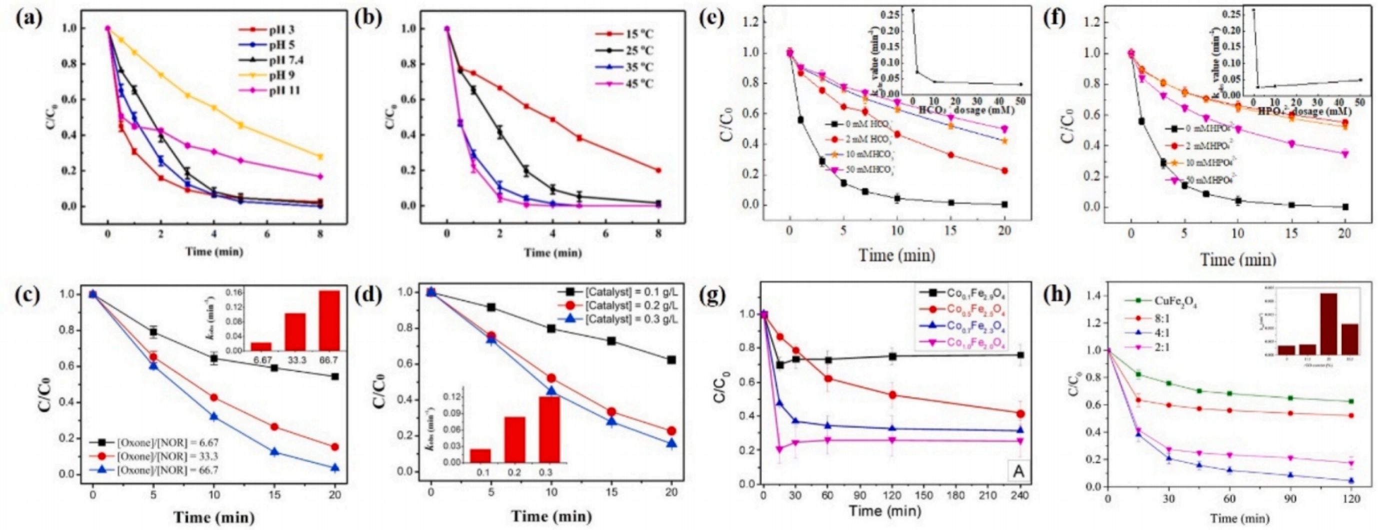

Fig. 9. Effects of different factors on catalyst performance and PMS activation: (a) pH and (b) temperature (Li et al., 2020), Copyright 2020 Elsevier. (c) PMS concentration and (d) catalyst dosage (Chen et al., 2018a, 2018b), Copyright 2018 Elsevier. (e) HCO_3^{-} and (f) HPO_4^{2-} (Xu et al., 2019), Copyright 2019 Elsevier. (g) different cobalt content in $Co_xFe_{3-x}O_4$ (Al-Anazi et al., 2018), Copyright 2018 Elsevier. (h) the mass ratio of $CuFe_2O_4$ to rGO (Hao et al., 2020), Copyright 2020 Elsevier. All reactions are carried out when other factors are at their optimum values.

reaction efficiency. Increasing the temperature can often significantly improve the degradation rate and shorten the reaction time (shown in Fig. 9b). High temperature is also one of the ways to promote the decomposition of PS into $SO_4^{-}\bullet$. However, some studies have shown that the catalytic efficiency decreases when the temperature is too high (Zhao et al., 2018; Wu et al., 2019), which may be related to the increased probability of radical recombination and the reaction of metal ions with $SO_4^{-}\bullet$ at high temperature. In fact, considering the practical application, the reaction system is generally carried out at room temperature (about 25 °C), rather than the optimal temperature obtained in the experiment. This is since the optimum temperature tends to be high and difficult to operate.

Moreover, different calcination temperatures lead to different spinel structures, which affect the catalytic performance. Bao et al. (2018) investigated the effect of calcination temperature on $CoFe_2O_4$ formation and properties. At a lower calcination temperature, NPs with a smaller particle size have a larger surface area, which can provide more active sites to generate more radicals. High calcination temperature can change the crystal structure, the degradation efficiency decreased with the increase of calcination temperature. Different MFe_2O_4 have various optimal calcination temperatures. The study by Deng et al. (2013) found that the $CoFe_2O_4$ obtained at a calcination temperature of 300 °C had the best catalytic activity.

3.3. PMS concentration and catalyst dosage

In this regard, it is generally believed by scholars that the increase of PMS concentration is beneficial to provide more $SO_4^{-}\bullet$, promoting the degradation reaction and improving the degradation efficiency (Zhao et al., 2014; Ji et al., 2015) (shown in Fig. 9c). Moreover, there is also an optimal amount of PMS concentration. Once the optimum concentration is exceeded, it causes a self-quenching reaction (Eq. (16)), which will clear itself or consume the remaining PMS, reducing the reaction efficiency (Amasha et al., 2018).

$$SO_4^{-}\bullet + HSO_5^{-} \rightarrow SO_5^{-}\bullet + HSO_4^{-} \tag{16}$$

The dosage of MFe_2O_4 NPs and NCs should also be selected appropriately to match the PMS concentration. Increasing the dosage can provide more active sites, producing more active radicals and speeding up the reaction rate (shown in Fig. 9d). In addition, for metal-doped catalysts with porous structures, too high doping dosage will cause pore blockage, resulting in a decrease in surface area and pore volume, which reduces the reaction efficiency.

3.4. Anions

The presence of anions in water can react with reactive oxygen species (ROS) and have a scavenging effect on radicals to quench them, affecting the catalytic performance. Cl^{-} is widely present in wastewater (Wang et al., 2011). It has the potential to react with ROS, thereby inhibiting the smooth progress of the reaction of MFe_2O_4 NPs and NCs/PMS system (Eq. (17)-Eq. (19)). In most cases, CO_3^{2-}, HCO_3^{-}, HPO_4^{2-} and $H_2PO_4^{-}$ all have a negative effect on the degradation reaction (Waldemer et al., 2007; Vicente et al., 2011). Fig. 9e and f show the effects of HCO_3^{-} and HPO_4^{2-} on the degradation of SMX. In particular, HPO_4^{2-} and $H_2PO_4^{-}$ can not only quench radicals but also chelate metal oxides. Their reactions with $SO_4^{-}\bullet$ or $\bullet OH$ are shown in Eq. (20)-Eq. (24). However, there is evidence that CO_3^{2-}, HCO_3^{-} and HPO_4^{2-} can effectively activate persulfate and play a positive role in the degradation process (Yang et al., 2010).

$$SO_4^{-}\bullet + Cl^{-} \rightarrow SO_4^{2-} + Cl\bullet \tag{17}$$

$$\bullet OH + Cl^{-} \rightarrow HOCl^{-}\bullet \tag{18}$$

$$HOCl^{-}\bullet + H^{+} \rightarrow Cl\bullet + H_2O \tag{19}$$

$$SO_4^{-}\bullet + CO_3^{2-} \rightarrow CO_3^{-}\bullet + SO_4^{2-} \tag{20}$$

$$SO_4^{-}\bullet + HCO_3^{-} \rightarrow HCO_3\bullet + SO_4^{2-} \tag{21}$$

$$\bullet OH + HCO_3^{-} \rightarrow CO_3^{2-} + H_2O \tag{22}$$

$$\bullet OH + HPO_4^{2-} \rightarrow HPO_4^{-}\bullet + OH^{-} \tag{23}$$

$$\bullet OH + H_2PO_4^{-} \rightarrow H_2PO_4\bullet + OH^{-} \tag{24}$$

3.5. The ratio of different components

The ratio of different metals plays a vital role in the structure and performance of MFe_2O_4 NPs. Due to the different activities of metals, the ratio of each metal will affect the overall effect of the catalyst when diverse kinds of metals are combined (shown in Fig. 9g). Chen et al. (2018a,b) observed that the structure of $Co_xFe_{3-x}O_4$ would transform from normal spinel into inverse spinel with the increases of x, resulting in the emergence of new active sites. To some extent, the Co content is directly proportional to the removal performance. However, whether higher Co content affects the properties of the final product is largely unknown. A similar result was reported by Su et al. (2013), who investigated the performance of $Co_xFe_{3-x}O_4$ on PMS activation and found that the presence of Co in the spinel structure is conducive to the decomposition of organic pollutants. As the increase of Co content, the reaction rate increased.

As for MFe_2O_4 NCs, the ratio of support to MFe_2O_4 will also affect the overall effect of catalyst, and there is an optimal value. Hao et al. (Hao et al., 2020) investigated the effect of graphene content in $CuFe_2O_4$-rGO on the degradation process and found the degradation efficiency increased first and then decreased with the increase of rGO content in NCs (shown in Fig. 9h). This may be related to the aggregation phenomenon caused by the high magnetic $CuFe_2O_4$ NPs content, which leads to the reduction of specific surface areas and affects the catalytic performance.

4. Conclusion and perspectives

SR-AOPs are a kind of advanced oxidation processes with great potential and prospect in the removal of organic pollutants. The introduction of metals has made great progress in the heterogeneous system for PMS activation. Single metal catalysts as activators for PMS activation gradually expose some defects in practical application. Hence, activators with polymetallic elements have been extensively and deeply studied in SR-AOPs. Spinel ferrite NPs not only have excellent catalytic performance and stability but also have strong ferrimagnetism, which makes them easy to recover from the reaction system. By fixing them on the support and synthesizing spinel ferrite NCs, the performance can be further enhanced and the self-agglomeration of magnetic NPs can be alleviated. A variety of superiorities make spinel ferrite NPs and their NCs ideal activator for PMS activation to remove organic pollutants. In this paper, research progress on PMS activation induced by typical spinel ferrite NPs and their NCs for organic pollutants removal are summarized, revealing the outstanding advantages and application potential of them. To improve the technology and strengthen the practical application, several aspects of spinel ferrite NPs and their NCs in SR-AOPs are worthy of in-depth discussion and investigation:

4.1. Ideal and reality

Up to now, most of the research is based on simulations and carried out under ideal conditions in the laboratory. It is not clear whether spinel ferrite NPs and their NCs work as well in practice as they do in the laboratory. Thus, more consideration should be given to the influence of actual environmental conditions on properties and the degradation effect. This is an area that needs to be explored and researched to prove that MFe_2O_4 NPs and NCs/PMS system has the potential of application from laboratory to industrial scale. In practice, for purpose of effectively removing organic pollutants, it is generally necessary to add a large number of PMS, resulting in the treated wastewater containing more sulfate ions. Current approaches to this problem are with the help of ion exchange or membrane processes to remove the residual sulfate anions before the wastewater is discharged into the environment, but this strategy increases processing costs. In addition, although studies have shown that spinel ferrite NPs and their NCs have good stability and a very low level of leaching, the ion leaching problem is still inevitable. Metal-containing sludge may become a new source of metals after proper recovery and treatment to further realize sustainable development and a virtuous cycle.

4.2. Performance improvement and cost consideration

The self-agglomeration of magnetic NPs results in the loss of accessible active sites. Scholars have focused on regulating the interatomic force of metal atoms in the synthesis process and developed a variety of technologies to prevent agglomeration or disperse agglomerated NPs, such as atomic layer deposition and pyrolysis strategies. It should be noted that it is effective to avoid agglomeration by means of supports, but the choice of support type will have an impact on the cost of the catalyst. For example, carbon-derived supports are normally expensive, which impedes their large-scale application in practice. Choosing cost-effective materials (such as natural minerals) for support is strongly encouraged. Furthermore, reasonable recovery and utilization of water treatment residuals and sludge-derived supports are also the focus of attention. Resource recycling and sustainable development are important issues of global concern.

4.3. Multi-technology combination

It is an effective way to save cost and improve efficiency to develop the multi-technology combination. Nowadays, there have been many pieces of research that combine SR-AOPs with ozone oxidation, photocatalysis, or irradiation technology. The rational use of external energy is a fresh research direction. In SR-AOPs, it is a brand-new method to cooperate spinel ferrite NPs and their NCs with UV or microwave. Moreover, the synergistic mechanism of hybrid systems is worth further study to be better applied in practice.

4.4. Emerging areas of application

Spinel ferrite NPs and their NCs have been successfully applied to remove organic pollutants from wastewater. Over the years, in-situ remediation of soil and groundwater has gradually become an emerging area of concern. At the same time, the treatment of landfill leachate and medical concentrated waste liquid also deserves more attention. It has been proved that spinel ferrite NPs and their NCs/PS system can play a positive role in landfill leachate degradation.

4.5. Selection and adjustment of activation pathways

SR-AOPs based on radical pathways have great mineralization ability to organic pollutants. However, the natural organic matter and anions present in the actual water environment will consume radicals, resulting in a greatly reduced in its actual degradation ability. On the contrary, SR-AOPs based on non-radical pathways have strong resistance to the interference of various natural organic matters and anions, but the mineralization rate of organic pollutants is not high enough. In consequence, for different water quality and organic pollutants, reasonable adjustment and precise selection of activation pathways are very necessary.

Declaration of competing interest

The authors declare that they have no known competing financial interests or personal relationships that could have appeared to influence the work reported in this paper.

Acknowledgments

The study was financially supported by the National Natural Science Foundation of China (51979103, 51679085), the Program for Changjiang Scholars and Innovative Research Team in University (IRT-13R17), the Funds of Hunan Science and Technology Innovation Project (2018RS3115, 2020RC5012), the Key Research and Development Project of Hunan Province of China (2017SK2241), the Project funded by China Postdoctoral Science Foundation (2021T140192, 2021M690054).

References

Ahn, Y.-Y., Yun, E.-T., Seo, J.-W., Lee, C., Kim, S.H., Kim, J.-H., Lee, J., 2016. Activation of peroxymonosulfate by surface-loaded noble metal nanoparticles for oxidative degradation of organic compounds. Environ. Sci. Technol. 50 (18), 10187–10197.

Al-Anazi, A., Abdelraheem, W.H., Han, C., Nadagouda, M.N., Sygellou, L., Arfanis, M.K., Falaras, P., Sharma, V.K., Dionysiou, D.D., 2018. Cobalt ferrite nanoparticles with controlled composition-peroxymonosulfate mediated degradation of 2-phenylbenzimidazole-5-sulfonic acid. Appl. Catal. B Environ. 221, 266–279.

Amasha, M., Baalbaki, A., Ghauch, A., 2018. A comparative study of the common persulfate activation techniques for the complete degradation of an NSAID: the case of ketoprofen. Chem. Eng. J. 350, 395–410.

Bao, Y., Lim, T.-T., Wang, R., Webster, R.D., Hu, X., 2018. Urea-assisted one-step synthesis of cobalt ferrite impregnated ceramic membrane for sulfamethoxazole degradation via peroxymonosulfate activation. Chem. Eng. J. 343, 737–747.

Benson, S.W., 1978. Thermochemistry and kinetics of sulfur-containing molecules and radicals. Chem. Rev. 78 (1), 23–35.

Bhat, A.P., Gogate, P.R., 2021. Degradation of nitrogen-containing hazardous compounds using advanced oxidation processes: a review on aliphatic and aromatic amines, dyes, and pesticides. J. Hazard Mater. 403, 123657.

Bie, C., Yu, H., Cheng, B., Ho, W., Fan, J., Yu, J., 2021. Design, fabrication, and mechanism of nitrogen-doped graphene-based photocatalyst. Adv. Mater. 33 (9), 2003521.

Cai, C., Kang, S., Xie, X., Liao, C., Duan, X., Dionysiou, D.D., 2020. Efficient degradation of bisphenol A in water by heterogeneous activation of peroxymonosulfate using highly active cobalt ferrite nanoparticles. J. Hazard Mater. 399, 122979.

Chan, K.H., Chu, W., 2009. Degradation of atrazine by cobalt-mediated activation of peroxymonosulfate: different cobalt counteranions in homogenous process and cobalt oxide catalysts in photolytic heterogeneous process. Water Res. 43 (9), 2513–2521.

Chen, G., Yu, Y., Liang, L., Duan, X., Li, R., Lu, X., Yan, B., Li, N., Wang, S., 2021. Remediation of antibiotic wastewater by coupled photocatalytic and persulfate oxidation system: a critical review. J. Hazard Mater. 408, 124461.

Chen, L., Ding, D., Liu, C., Cai, H., Qu, Y., Yang, S., Gao, Y., Cai, T., 2018a. Degradation of norfloxacin by $CoFe_2O_4$-GO composite coupled with peroxymonosulfate: a comparative study and mechanistic consideration. Chem. Eng. J. 334, 273–284.

Chen, L., Zuo, X., Zhou, L., Huang, Y., Yang, S., Cai, T., Ding, D., 2018b. Efficient heterogeneous activation of peroxymonosulfate by facilely prepared Co/Fe bimetallic oxides: kinetics and mechanism. Chem. Eng. J. 345, 364–374.

Deng, J., Shao, Y., Gao, N., Tan, C., Zhou, S., Hu, X., 2013. $CoFe_2O_4$ magnetic nanoparticles as a highly active heterogeneous catalyst of oxone for the degradation of diclofenac in water. J. Hazard Mater. 262, 836–844.

Ding, Y., Zhu, L., Wang, N., Tang, H., 2013. Sulfate radicals induced degradation of tetrabromobisphenol A with nanoscaled magnetic $CuFe_2O_4$ as a heterogeneous catalyst of peroxymonosulfate. Appl. Catal. B Environ. 129, 153–162.

Dong, X., Ren, B., Sun, Z., Li, C., Zhang, X., Kong, M., Zheng, S., Dionysiou, D.D., 2019. Monodispersed $CuFe_2O_4$ nanoparticles anchored on natural kaolinite as highly efficient peroxymonosulfate catalyst for bisphenol A degradation. Appl. Catal. B Environ. 253, 206–217.

Du, Y., Ma, W., Liu, P., Zou, B., Ma, J., 2016. Magnetic $CoFe_2O_4$ nanoparticles supported on titanate nanotubes ($CoFe_2O_4$/TNTs) as a novel heterogeneous catalyst for peroxymonosulfate activation and degradation of organic pollutants. J. Hazard Mater. 308, 58–66.

Duan, X., Sun, H., Kang, J., Wang, Y., Indrawirawan, S., Wang, S., 2015. Insights into heterogeneous catalysis of persulfate activation on dimensional-structured nanocarbons. ACS Catal. 5 (8), 4629–4636.

Fang, G.-D., Dionysiou, D.D., Al-Abed, S.R., Zhou, D.-M., 2013. Superoxide radical driving the activation of persulfate by magnetite nanoparticles: implications for the degradation of PCBs. Appl. Catal. B Environ. 129, 325–332.

Fu, H., Ma, S., Zhao, P., Xu, S., Zhan, S., 2019. Activation of peroxymonosulfate by graphitized hierarchical porous biochar and $MnFe_2O_4$ magnetic nanoarchitecture for organic pollutants degradation: structure dependence and mechanism. Chem. Eng. J. 360, 157–170.

Giannakis, S., Lin, K.-Y.A., Ghanbari, F., 2021. A review of the recent advances on the treatment of industrial wastewaters by Sulfate Radical-based Advanced Oxidation Processes (SR-AOPs). Chem. Eng. J. 406, 127083.

Golshan, M., Kakavandi, B., Ahmadi, M., Azizi, M., 2018. Photocatalytic activation of peroxymonosulfate by TiO_2 anchored on cupper ferrite (TiO_2@$CuFe_2O_4$) into 2,4-D degradation: process feasibility, mechanism and pathway. J. Hazard Mater. 359, 325–337.

Guan, Y.H., Ma, J., Ren, Y.M., Liu, Y.L., Xiao, J.Y., Lin, L.Q., Zhang, C., 2013. Efficient degradation of atrazine by magnetic porous copper ferrite catalyzed peroxymonosulfate oxidation via the formation of hydroxyl and sulfate radicals. Water Res. 47 (14), 5431–5438.

Guo, Q., Zhou, C., Ma, Z., Yang, X., 2019. Fundamentals of TiO_2 photocatalysis: concepts, mechanisms, and challenges. Adv. Mater. 31 (50), 1901997.

Hao, P., Hu, M., Xing, R., Zhou, W., 2020. Synergistic degradation of methylparaben on $CuFe_2O_4$-rGO composite by persulfate activation. J. Alloys Compd. 823, 153757.

Harris, V.G., Geiler, A., Chen, Y., Yoon, S.D., Wu, M., Yang, A., Chen, Z., He, P., Parimi, P. V., Zuo, X., Patton, C.E., Abe, M., Acher, O., Vittoria, C., 2009. Recent advances in processing and applications of microwave ferrites. J. Magn. Magn Mater. 321 (14), 2035–2047.

Hu, P., Long, M., 2016. Cobalt-catalyzed sulfate radical-based advanced oxidation: a review on heterogeneous catalysts and applications. Appl. Catal. B Environ. 181, 103–117.

Ike, I.A., Linden, K.G., Orbell, J.D., Duke, M., 2018. Critical review of the science and sustainability of persulphate advanced oxidation processes. Chem. Eng. J. 338, 651–669.

Jawad, A., Lang, J., Liao, Z., Khan, A., Ifthikar, J., Lv, Z., Long, S., Chen, Z., Chen, Z., 2018. Activation of persulfate by CuO_x@Co-LDH: a novel heterogeneous system for contaminant degradation with broad pH window and controlled leaching. Chem. Eng. J. 335, 548–559.

Ji, Y., Dong, C., Kong, D., Lu, J., Zhou, Q., 2015. Heat-activated persulfate oxidation of atrazine: implications for remediation of groundwater contaminated by herbicides. Chem. Eng. J. 263, 45–54.

Karimipourfard, D., Eslamloueyan, R., Mehranbod, N., 2019. Novel heterogeneous degradation of mature landfill leachate using persulfate and magnetic $CuFe_2O_4$/RGO nanocatalyst. Process Saf. Environ. Protect. 131, 212–222.

Karimipourfard, D., Eslamloueyan, R., Mehranbod, N., 2020. Heterogeneous degradation of stabilized landfill leachate using persulfate activation by $CuFe_2O_4$ nanocatalyst: an experimental investigation. J. Environ. Chem. Eng. 8 (2), 103426.

Kefeni, K.K., Mamba, B.B., Msagati, T.A.M., 2017. Application of spinel ferrite nanoparticles in water and wastewater treatment: a review. Separ. Purif. Technol. 188, 399–422.

Kolthoff, I.M., Miller, I.K., 1951. The chemistry of persulfate. I. The kinetics and mechanism of the decomposition of the persulfate ion in aqueous Medium1. J. Am. Chem. Soc. 73 (7), 3055–3059.

Lang, X., Chen, X., Zhao, J., 2014. Heterogeneous visible light photocatalysis for selective organic transformations. Chem. Soc. Rev. 43 (1), 473–486.

Laokul, P., Amornkitbamrung, V., Seraphin, S., Maensiri, S., 2011. Characterization and magnetic properties of nanocrystalline $CuFe_2O_4$, $NiFe_2O_4$, $ZnFe_2O_4$ powders prepared by the Aloe vera extract solution. Curr. Appl. Phys. 11 (1), 101–108.

Lei, Y., Chen, C.-S., Tu, Y.-J., Huang, Y.-H., Zhang, H., 2015. Heterogeneous degradation of organic pollutants by persulfate activated by CuO-Fe_3O_4: mechanism, stability, and effects of pH and bicarbonate ions. Environ. Sci. Technol. 49 (11), 6838–6845.

Li, C., Huang, Y., Dong, X., Sun, Z., Duan, X., Ren, B., Zheng, S., Dionysiou, D.D., 2019. Highly efficient activation of peroxymonosulfate by natural negatively-charged kaolinite with abundant hydroxyl groups for the degradation of atrazine. Appl. Catal. B Environ. 247, 10–23.

Li, C., Sun, Z., Zhang, W., Yu, C., Zheng, S., 2018. Highly efficient g-C_3N_4/TiO_2/kaolinite composite with novel three-dimensional structure and enhanced visible light responding ability towards ciprofloxacin and S. aureus. Appl. Catal. B Environ. 220, 272–282.

Li, J., Xu, M., Yao, G., Lai, B., 2018. Enhancement of the degradation of atrazine through $CoFe_2O_4$ activated peroxymonosulfate (PMS) process: kinetic, degradation intermediates, and toxicity evaluation. Chem. Eng. J. 348, 1012–1024.

Li, X., Liu, X., Lin, C., Zhang, H., Zhou, Z., Fan, G., Ma, J., 2019. Cobalt ferrite nanoparticles supported on drinking water treatment residuals: an efficient magnetic heterogeneous catalyst to activate peroxymonosulfate for the degradation of atrazine. Chem. Eng. J. 367, 208–218.

Li, X., Zhang, D., Liu, Z., Lyu, C., Niu, S., Dong, Z., Lyu, C., 2020. Enhanced catalytic oxidation of benzotriazole via peroxymonosulfate activated by $CoFe_2O_4$ supported onto nitrogen-doped three-dimensional graphene aerogels. Chem. Eng. J. 400, 125897.

Li, Y., Ma, S., Xu, S., Fu, H., Li, Z., Li, K., Sheng, K., Du, J., Lu, X., Li, X., Liu, S., 2020. Novel magnetic biochar as an activator for peroxymonosulfate to degrade bisphenol A: emphasizing the synergistic effect between graphitized structure and $CoFe_2O_4$. Chem. Eng. J. 387, 124094.

Liang, C., Wang, Z.-S., Bruell, C.J., 2007. Influence of pH on persulfate oxidation of TCE at ambient temperatures. Chemosphere 66 (1), 106–113.

Liang, Y., Li, H., 2017. A comparison of trimeric surfactant intercalated montmorillonite with its gemini modified one: characterization and application in methyl orange removal. J. Mol. Liq. 227, 139–146.

Liu, H., Bruton, T.A., Li, W., Buren, J.V., Prasse, C., Doyle, F.M., Sedlak, D.L., 2016. Oxidation of benzene by persulfate in the presence of Fe(III)- and Mn(IV)-Containing oxides: stoichiometric efficiency and transformation products. Environ. Sci. Technol. 50 (2), 890–898.

Liu, L., Mi, H., Zhang, M., Sun, F., Zhan, R., Zhao, H., He, S., Zhou, L., 2021. Efficient moxifloxacin degradation by $CoFe_2O_4$ magnetic nanoparticles activated peroxymonosulfate: kinetics, pathways and mechanisms. Chem. Eng. J. 407, 127201.

Lu, L., Gao, M., Gu, Z., Yang, S., Liu, Y., 2014. A comparative study and evaluation of sulfamethoxazole adsorption onto organo-montmorillonites. J. Environ. Sci. 26 (12), 2535–2545.

Lyu, J., Ge, M., Hu, Z., Guo, C., 2020. One-pot synthesis of magnetic CuO/Fe_2O_3/$CuFe_2O_4$ nanocomposite to activate persulfate for levofloxacin removal: investigation of efficiency, mechanism and degradation route. Chem. Eng. J. 389, 124456.

Ma, Q., Nengzi, L.-c., Zhang, X., Zhao, Z., Cheng, X., 2020. Enhanced activation of persulfate by AC@$CoFe_2O_4$ nanocomposites for effective removal of lomefloxacin. Separ. Purif. Technol. 233, 115978.

Ma, Q., Zhang, H., Zhang, X., Li, B., Guo, R., Cheng, Q., Cheng, X., 2019. Synthesis of magnetic CuO/$MnFe_2O_4$ nanocompisite and its high activity for degradation of levofloxacin by activation of persulfate. Chem. Eng. J. 360, 848–860.

Mukhopadhyay, R., Bhaduri, D., Sarkar, B., Rusmin, R., Hou, D., Khanam, R., Sarkar, S., Kumar Biswas, J., Vithanage, M., Bhatnagar, A., Ok, Y.S., 2020. Clay-polymer nanocomposites: progress and challenges for use in sustainable water treatment. J. Hazard Mater. 383, 121125.

Oh, W.-D., Dong, Z., Lim, T.-T., 2016. Generation of sulfate radical through heterogeneous catalysis for organic contaminants removal: current development, challenges and prospects. Appl. Catal. B Environ. 194, 169–201.

Pan, X., Yan, L., Li, C., Qu, R., Wang, Z., 2017. Degradation of UV-filter benzophenone-3 in aqueous solution using persulfate catalyzed by cobalt ferrite. Chem. Eng. J. 326, 1197–1209.

Pan, Y., Liu, X., Zhang, W., Liu, Z., Zeng, G., Shao, B., Liang, Q., He, Q., Yuan, X., Huang, D., Chen, M., 2020. Advances in photocatalysis based on fullerene C_{60} and its derivatives: properties, mechanism, synthesis, and applications. Appl. Catal. B Environ. 265, 118579.

Pang, Y., Lei, H., 2016. Degradation of p-nitrophenol through microwave-assisted heterogeneous activation of peroxymonosulfate by manganese ferrite. Chem. Eng. J. 287, 585–592.

Peng, Y., Tang, H., Yao, B., Gao, X., Yang, X., Zhou, Y., 2021. Activation of peroxymonosulfate (PMS) by spinel ferrite and their composites in degradation of organic pollutants: a Review. Chem. Eng. J. 414, 128800.

Peng, Z., Liu, X., Zhang, W., Zeng, Z., Liu, Z., Zhang, C., Liu, Y., Shao, B., Liang, Q., Tang, W., Yuan, X., 2020. Advances in the application, toxicity and degradation of carbon nanomaterials in environment: a review. Environ. Int. 134, 105298.

Reddy, D.H.K., Yun, Y.-S., 2016. Spinel ferrite magnetic adsorbents: alternative future materials for water purification? Coord. Chem. Rev. 315, 90–111.

Ren, Y., Lin, L., Ma, J., Yang, J., Feng, J., Fan, Z., 2015. Sulfate radicals induced from peroxymonosulfate by magnetic ferrospinel MFe_2O_4 (M = Co, Cu, Mn, and Zn) as heterogeneous catalysts in the water. Appl. Catal. B Environ. 165, 572–578.

Rizzo, L., 2011. Bioassays as a tool for evaluating advanced oxidation processes in water and wastewater treatment. Water Res. 45 (15), 4311–4340.

Senapati, K.K., Borgohain, C., Phukan, P., 2011. Synthesis of highly stable $CoFe_2O_4$ nanoparticles and their use as magnetically separable catalyst for Knoevenagel reaction in aqueous medium. J. Mol. Catal. Chem. 339 (1–2), 24–31.

Shao, B., Liu, Z., Zeng, G., Liu, Y., Liang, Q., He, Q., Wu, T., Pan, Y., Huang, J., Peng, Z., Luo, S., Liang, C., Liu, X., Tong, S., Liang, J., 2021. Synthesis of 2D/2D CoAl-LDHs/$Ti_3C_2T_x$ Schottky-junction with enhanced interfacial charge transfer and visible-light photocatalytic performance. Appl. Catal. B Environ. 286, 119867.

Shao, B., Liu, Z., Zeng, G., Wang, H., Liang, Q., He, Q., Cheng, M., Zhou, C., Jiang, L., Song, B., 2020. Two-dimensional transition metal carbide and nitride (MXene) derived quantum dots (QDs): synthesis, properties, applications and prospects. J. Mater. Chem. 8 (16), 7508–7535.

Su, S., Guo, W., Leng, Y., Yi, C., Ma, Z., 2013. Heterogeneous activation of Oxone by $Co_{(x)}Fe_{(3-x)}O_4$ nanocatalysts for degradation of rhodamine B. J. Hazard Mater. 244–245, 736–742.

Takdastan, A., Kakavandi, B., Azizi, M., Golshan, M., 2018. Efficient activation of peroxymonosulfate by using ferroferric oxide supported on carbon/UV/US system: a new approach into catalytic degradation of bisphenol A. Chem. Eng. J. 331, 729–743.

Tan, C., Gao, N., Fu, D., Deng, J., Deng, L., 2017. Efficient degradation of paracetamol with nanoscaled magnetic $CoFe_2O_4$ and $MnFe_2O_4$ as a heterogeneous catalyst of peroxymonosulfate. Separ. Purif. Technol. 175, 47–57.

Tian, W., Zhang, H., Qian, Z., Ouyang, T., Sun, H., Qin, J., Tadé, M.O., Wang, S., 2018. Bread-making synthesis of hierarchically Co@C nanoarchitecture in heteroatom doped porous carbons for oxidative degradation of emerging contaminants. Appl. Catal. B Environ. 225, 76–83.

Tsitonaki, A., Petri, B., Crimi, M., MosbÆK, H., Siegrist, R.L., Bjerg, P.L., 2010. In situ chemical oxidation of contaminated soil and groundwater using persulfate: a review. Crit. Rev. Environ. Sci. Technol. 40 (1), 55–91.

Vicente, F., Santos, A., Romero, A., Rodriguez, S., 2011. Kinetic study of diuron oxidation and mineralization by persulphate: effects of temperature, oxidant concentration and iron dosage method. Chem. Eng. J. 170 (1), 127–135.

Wacławek, S., Lutze, H.V., Grübel, K., Padil, V.V.T., Černík, M., Dionysiou, D.D., 2017. Chemistry of persulfates in water and wastewater treatment: a review. Chem. Eng. J. 330, 44–62.

Waldemer, R.H., Tratnyek, P.G., Johnson, R.L., Nurmi, J.T., 2007. Oxidation of chlorinated ethenes by heat-activated persulfate: kinetics and products. Environ. Sci. Technol. 41 (3), 1010–1015.

Wang, J., Chen, H., 2020. Catalytic ozonation for water and wastewater treatment: recent advances and perspective. Sci. Total Environ. 704, 135249.

Wang, L., Li, J., Wang, Y., Zhao, L., Jiang, Q., 2012. Adsorption capability for Congo red on nanocrystalline MFe_2O_4 (M = Mn, Fe, Co, Ni) spinel ferrites. Chem. Eng. J. 181–182, 72–79.

Wang, Q., Shao, Y., Gao, N., Chu, W., Chen, J., Lu, X., Zhu, Y., An, N., 2017. Activation of peroxymonosulfate by Al_2O_3-based $CoFe_2O_4$ for the degradation of sulfachloropyridazine sodium: kinetics and mechanism. Separ. Purif. Technol. 189, 176–185.

Wang, Y., Zhao, H., Li, M., Fan, J., Zhao, G., 2014. Magnetic ordered mesoporous copper ferrite as a heterogeneous Fenton catalyst for the degradation of imidacloprid. Appl. Catal. B Environ. 147, 534–545.

Wang, Z., Yuan, R., Guo, Y., Xu, L., Liu, J., 2011. Effects of chloride ions on bleaching of azo dyes by Co2+/oxone regent: kinetic analysis. J. Hazard Mater. 190 (1), 1083–1087.

Wu, C., Chen, W., Gu, Z., Li, Q., 2021. A review of the characteristics of Fenton and ozonation systems in landfill leachate treatment. Sci. Total Environ. 762, 143131.

Wu, J., Cagnetta, G., Wang, B., Cui, Y., Deng, S., Wang, Y., Huang, J., Yu, G., 2019. Efficient degradation of carbamazepine by organo-montmorillonite supported $nCoFe_2O_4$-activated peroxymonosulfate process. Chem. Eng. J. 368, 824–836.

Wu, T., Liu, X., Liu, Y., Cheng, M., Liu, Z., Zeng, G., Shao, B., Liang, Q., Zhang, W., He, Q., Zhang, W., 2020. Application of QD-MOF composites for photocatalysis: energy production and environmental remediation. Coord. Chem. Rev. 403, 213097.

Xiao, K., Chen, S., Yang, B., Zhao, X., Yu, G., Zhu, C., 2019. Simultaneous achievement of refractory pollutant removal and energy production in the saline wastewater treatment. Chem. Eng. J. 369, 845–853.

Xiao, R., Luo, Z., Wei, Z., Luo, S., Spinney, R., Yang, W., Dionysiou, D.D., 2018. Activation of peroxymonosulfate/persulfate by nanomaterials for sulfate radical-based advanced oxidation technologies. Curr. Opin. Chem. Eng. 19, 51–58.

Xu, L.J., Chu, W., Gan, L., 2015. Environmental application of graphene-based $CoFe_2O_4$ as an activator of peroxymonosulfate for the degradation of a plasticizer. Chem. Eng. J. 263, 435–443.

Xu, M., Li, J., Yan, Y., Zhao, X., Yan, J., Zhang, Y., Lai, B., Chen, X., Song, L., 2019. Catalytic degradation of sulfamethoxazole through peroxymonosulfate activated with expanded graphite loaded $CoFe_2O_4$ particles. Chem. Eng. J. 369, 403–413.

Xu, Y., Ai, J., Zhang, H., 2016. The mechanism of degradation of bisphenol A using the magnetically separable $CuFe_2O_4$/peroxymonosulfate heterogeneous oxidation process. J. Hazard Mater. 309, 87–96.

Yang, J., Zhu, M., Dionysiou, D.D., 2021. What is the role of light in persulfate-based advanced oxidation for water treatment? Water Res. 189, 116627.

Yang, Q., Choi, H., Al-Abed, S.R., Dionysiou, D.D., 2009. Iron-cobalt mixed oxide nanocatalysts: heterogeneous peroxymonosulfate activation, cobalt leaching, and ferromagnetic properties for environmental applications. Appl. Catal. B Environ. 88 (3–4), 462–469.

Yang, Q., Ma, Y., Chen, F., Yao, F., Sun, J., Wang, S., Yi, K., Hou, L., Li, X., Wang, D., 2019. Recent advances in photo-activated sulfate radical-advanced oxidation process (SR-AOP) for refractory organic pollutants removal in water. Chem. Eng. J. 378, 122149.

Yang, S., Wang, C., Li, J., Yan, N., Ma, L., Chang, H., 2011. Low temperature selective catalytic reduction of NO with NH_3 over Mn-Fe spinel: performance, mechanism and kinetic study. Appl. Catal. B Environ. 110, 71–80.

Yang, S., Wang, P., Yang, X., Shan, L., Zhang, W., Shao, X., Niu, R., 2010. Degradation efficiencies of azo dye Acid Orange 7 by the interaction of heat, UV and anions with common oxidants: persulfate, peroxymonosulfate and hydrogen peroxide. J. Hazard Mater. 179 (1), 552–558.

Yang, Z., Li, Y., Zhang, X., Cui, X., He, S., Liang, H., Ding, A., 2020. Sludge activated carbon-based $CoFe_2O_4$-SAC nanocomposites used as heterogeneous catalysts for degrading antibiotic norfloxacin through activating peroxymonosulfate. Chem. Eng. J. 384, 123319.

Yao, C., Zhang, Y., Du, M., Du, X., Huang, S., 2019. Insights into the mechanism of non-radical activation of persulfate via activated carbon for the degradation of p-chloroaniline. Chem. Eng. J. 362, 262–268.

Yao, L., Yang, H., Chen, Z., Qiu, M., Hu, B., Wang, X., 2021. Bismuth oxychloride-based materials for the removal of organic pollutants in wastewater. Chemosphere 273, 128576.

Yao, Y., Cai, Y., Lu, F., Wei, F., Wang, X., Wang, S., 2014a. Magnetic recoverable $MnFe_2O_4$ and $MnFe_2O_4$-graphene hybrid as heterogeneous catalysts of peroxymonosulfate activation for efficient degradation of aqueous organic pollutants. J. Hazard Mater. 270, 61–70.

Yao, Y., Qin, J., Cai, Y., Wei, F., Lu, F., Wang, S., 2014b. Facile synthesis of magnetic $ZnFe_2O_4$-reduced graphene oxide hybrid and its photo-Fenton-like behavior under visible iradiation. Environ. Sci. Pollut. Control Ser. 21 (12), 7296–7306.

You, Y., Shi, Z., Li, Y., Zhao, Z., He, B., Cheng, X., 2021. Magnetic cobalt ferrite biochar composite as peroxymonosulfate activator for removal of lomefloxacin hydrochloride. Separ. Purif. Technol. 272, 118889.

Yu, J., Feng, H., Tang, L., Pang, Y., Zeng, G., Lu, Y., Dong, H., Wang, J., Liu, Y., Feng, C., Wang, J., Peng, B., Ye, S., 2020. Metal-free carbon materials for persulfate-based advanced oxidation process: microstructure, property and tailoring. Prog. Mater. Sci. 111, 100654.

Yuan, S., Liao, P., Alshawabkeh, A.N., 2014. Electrolytic manipulation of persulfate reactivity by iron electrodes for trichloroethylene degradation in groundwater. Environ. Sci. Technol. 48 (1), 656–663.

Zhang, H., Song, Y., Nengzi, L.-c., Gou, J., Li, B., Cheng, X., 2020. Activation of persulfate by a novel magnetic $CuFe_2O_4/Bi_2O_3$ composite for lomefloxacin degradation. Chem. Eng. J. 379, 122362.

Zhang, J., Su, D.S., Blume, R., Schlögl, R., Wang, R., Yang, X., Gajović, A., 2010. Surface chemistry and catalytic reactivity of a nanodiamond in the steam-free dehydrogenation of ethylbenzene. Angew. Chem. Int. Ed. 49 (46), 8640–8644.

Zhang, Q., Sun, X., Dang, Y., Zhu, J.-J., Zhao, Y., Xu, X., Zhou, Y., 2022. A novel electrochemically enhanced homogeneous PMS-heterogeneous $CoFe_2O_4$ synergistic catalysis for the efficient removal of levofloxacin. J. Hazard Mater. 424, 127651.

Zhang, T., Zhu, H., Croué, J.-P., 2013. Production of sulfate radical from peroxymonosulfate induced by a magnetically separable $CuFe_2O_4$ spinel in water: efficiency, stability, and mechanism. Environ. Sci. Technol. 47 (6), 2784–2791.

Zhang, X., Feng, M., Qu, R., Liu, H., Wang, L., Wang, Z., 2016. Catalytic degradation of diethyl phthalate in aqueous solution by persulfate activated with nano-scaled magnetic $CuFe_2O_4$/MWCNTs. Chem. Eng. J. 301, 1–11.

Zhang, X., Feng, M., Wang, L., Qu, R., Wang, Z., 2017. Catalytic degradation of 2-phenylbenzimidazole-5-sulfonic acid by peroxymonosulfate activated with nitrogen and sulfur co-doped CNTs-COOH loaded $CuFe_2O_4$. Chem. Eng. J. 307, 95–104.

Zhao, L., Hou, H., Fujii, A., Hosomi, M., Li, F., 2014. Degradation of 1,4-dioxane in water with heat- and Fe^{2+}-activated persulfate oxidation. Environ. Sci. Pollut. Control Ser. 21 (12), 7457–7465.

Zhao, Y., Ma, X., Xu, P., Wang, H., Liu, Y., He, A., 2018. Elemental mercury removal from flue gas by $CoFe_2O_4$ catalyzed peroxymonosulfate. J. Hazard Mater. 341, 228–237.

Zhao, Y., Song, M., Cao, Q., Sun, P., Chen, Y., Meng, F., 2020. The superoxide radicals' production via persulfate activated with $CuFe_2O_4$@Biochar composites to promote the redox pairs cycling for efficient degradation of o-nitrochlorobenzene in soil. J. Hazard Mater. 400, 122887.

Zhou, Y., Xiang, Y., He, Y., Yang, Y., Zhang, J., Luo, L., Peng, H., Dai, C., Zhu, F., Tang, L., 2018. Applications and factors influencing of the persulfate-based advanced oxidation processes for the remediation of groundwater and soil contaminated with organic compounds. J. Hazard Mater. 359, 396–407.